# Analysis of the 2002 Mw = 7.6 Wewak Earthquake, Papua New Guinea, using Global Positioning System Observations

**Ryan Ruddick**

**A thesis submitted for the degree of**
**Honours in Physics of the Earth**
**at the**
**The Australian National University**

**October, 2005**

# Declaration

This thesis is an account of research undertaken between Feburary 2005 and October 2005 at the Research School of Earth Sciences, The Australian National University, Canberra, Australia.

Except where acknowledged in the customary manner, the material presented in this thesis is, to the best of my knowledge, original and has not been submitted in whole or part for a degree in any university.

Ryan Ruddick

October, 2005

# Acknowledgements

Firstly, I would like to thank my supervisor, Paul Tregoning, who not only suggested the topic of this thesis, but patiently answered my questions and always pointed me in the right direction, whether I saw it at the time or not. I also want to extend my thanks to Herb for reminding me to back up my data (I should have taken more notice!), to Richard for his insights on Papua New Guinea's tectonics, to Gisela for letting me share her office and for not complaining about the wall of papers I surrounded myself with, to Richie and all those who collected and organised the GPS data from PNG, and to everyone at the Research School of Earth Sciences who made me feel welcome. I am further grateful to David Tappin of the British Geological Survey who allowed me access to his bathymetry data from Papua New Guinea.

I extend my gratitude to the staff at the Centre for Spatial Information Science at UTAS, who helped me develop a passion for spatial science. In particular I want to thank Jon Osborn and Richard Coleman, who provided me with many references and helped with applications. If it were not for the suggestion from Richard Coleman to undertake a Summer Scholarship at the ANU, I would without doubt, still be hammering stakes into the ground.

Without my friends and family, both in Tasmania and Canberra, this year would have been very different. I thank them all for their encouragement, kind words, and numerous yet much needed distractions. In particular I want to separately thank my mum and dad who, despite their lack of geophysical knowledge, still proof read many chapters for me. I want to thank Gemma, for her entertaining suggestions of additions to my thesis, I am still looking for a suitable place to add them. A big thankyou to my housemates Pat and Mary for their support and entertainment throughtout the year. Special thanks must also go to Anita, who despite her own problems, has provided me over the last five years, with un-parallelled support.

Finally, I would like to thank the Australian National University, for their generous scholarship, which helped make my move to Canberra significantly more enjoyable.

# Abstract

The 2002 $M_w$ = 7.6 Wewak earthquake ruputred the New Guinea Trench off the northern coast of Papua New Guinea. A survey conducted by the University of Papua New Guinea reports that consistent uplift of 30 - 40 cm occured across the near shore islands and localised subsidence of 10 - 20 cm occured near Hawain. The measurements are shown using an elastic dislocation model to be consistent with the Harvard CMT focal mechanism for the event ($\phi$ = 106°, $\delta$ = 34°, $\lambda$ = 43°). This study compares the previously published interpretation of the ruputre with Global Positioning System observations of co-seismic deformation.

GPS observations have been made since 2000, at 8 sites spanning the New Guinea Trench and Bismarck Sea Seismic Lineation. The GPS data were processed with the GAMIT/GLOBK software to estimate site positions relative to the ITRF2000. A time series analysis revealed clear co-seismic displacments corresponding to the time of the Wewak earthquake. By comparing estimated rigid plate motions for the area with estimated GPS velocities it was shown that the region is experiencing post-seismic relaxation across the New Guinea Trench and significant inter-seismic coupling across the Bismarck Sea Seismic Lineation.

The co-seismic displacements were inverted using the non-linear approach of the Neighbourhood Algorithm with an elastic dislocation model, to estimate fault geometry and slip parameters of a seismic ruputre. It is shown that the GPS displacements can be explained by a steeply dipping thrust fault. However, this model is not consistent with the reported values of uplift and subsidence. A second model shows that it is not possible to reconcile the observed uplift and subsidence with the horizontal co-seismic displacements using a single rupture model. Suggestion is made to a possible rupture which began on the New Guinea Trench west of Kairiru and propogated east in two stages.

# Contents

# List of Figures

# List of Tables

# Abbreviations

**ADL** Adelbert Block

**ANU** The Australian National University

**AUS** Australian Plate

**BSSL** Bismarck Sea Seismic Lineation

**ED** Elastic Dislocation Theory

**GAMIT** GPS At MIT

**GLOBK** GLOBal Kalman filter

**GPS** Global Positioning System

**Harvard CMT** Havard Central Moment Tensor

**IGS** International Global Navigation Satellite System Serivce

**ITRF** The International Terrestrial Reference Frame (usually at epoch 2000.)

**ITST** International Tsunami Survey Team

$\mathbf{M}_w$ Moment Magnitude

**MAN** Manus Plate

**NA** Neighbourhood Algorithm (*Sambridge*, 1999a,b)

**NBP** North Bismarck Plate

**NEIC** National Earthquake Information Center (see also USGS)

**NGH** New Guinea Highlands Block

**NGT** New Guinea Trench

**PAC** Pacific Plate

**PDE** Preliminary Determination of Epicenters (see also USGS)

**PNG** Papua New Guinea

**PNG98** 17 July 1998 Sissano Lagoon Earthquake and Tsunami

**PNG02** 8 September 2002 Wewak Earthquake and Tsunami

**SBP** South Bismarck Plate

**SS** Solomon Sea Plate

**TBD** Trobriand Plate

**UPNG** The University of Papua New Guinea

**USGS** The United States Geological Society

**UTC** Universal Coordinated Time

**WLK** Woodlark Plate

**VLBI** Very Long Baseline Interferometry

# Introduction

## 1.1 Overview

At 18:44 (UTC) on 8 September 2002 an earthquake of magnitude $M_w$ = 7.6 occurred off the northern coast of the East Sepik Province of Papua New Guinea (PNG), near the village of Wewak (Figure 1.1). The event, a low angle thrust (strike $\phi = 106°$, dip $\delta = 34°$, slip $\lambda = 43°$) (Harvard CMT Catalogue) triggered a moderate tsunami which was observed along 300 km of coast (*Borrero et al.*, 2003). Soon after the event a survey, conducted by the University of Papua New Guinea (UPNG) and the International Tsunami Survey Team (ITST), was undertaken to measure reef uplift, tsunami run-up and inundation. The results of this survey supported the Harvard CMT solution and *Borrero et al.* (2003) describe the event to be a "classic textbook seismic dislocation."

The aim of this study is to re-examine the 2002 Wewak earthquake and tsunami using geodetic data obtained from the Global Positioning System (GPS). The GPS provides a means by which positions can be determined with high precision, as such the tectonic setting of an area can be well described using site motions and strain rates. In this study I use GPS observations to describe the tectonic setting of the East Sepik region and estimate co-seismic displacements caused by the 2002 earthquake. The GPS estimated surface displacements do not match those derived from the Harvard CMT solution as assumed by *Borrero et al.* (2003) (Figure 1.1). Therefore the focus of study is to reconcile these conflicting datasets. In particular, I look at a method of inverting co-seismic displacements to estimate fault geometry and slip parameters. There is interest in this study as it provides a valuable description of the tectonic setting of PNG's northern coast, which is an area that is both under-studied and tectonically complex.

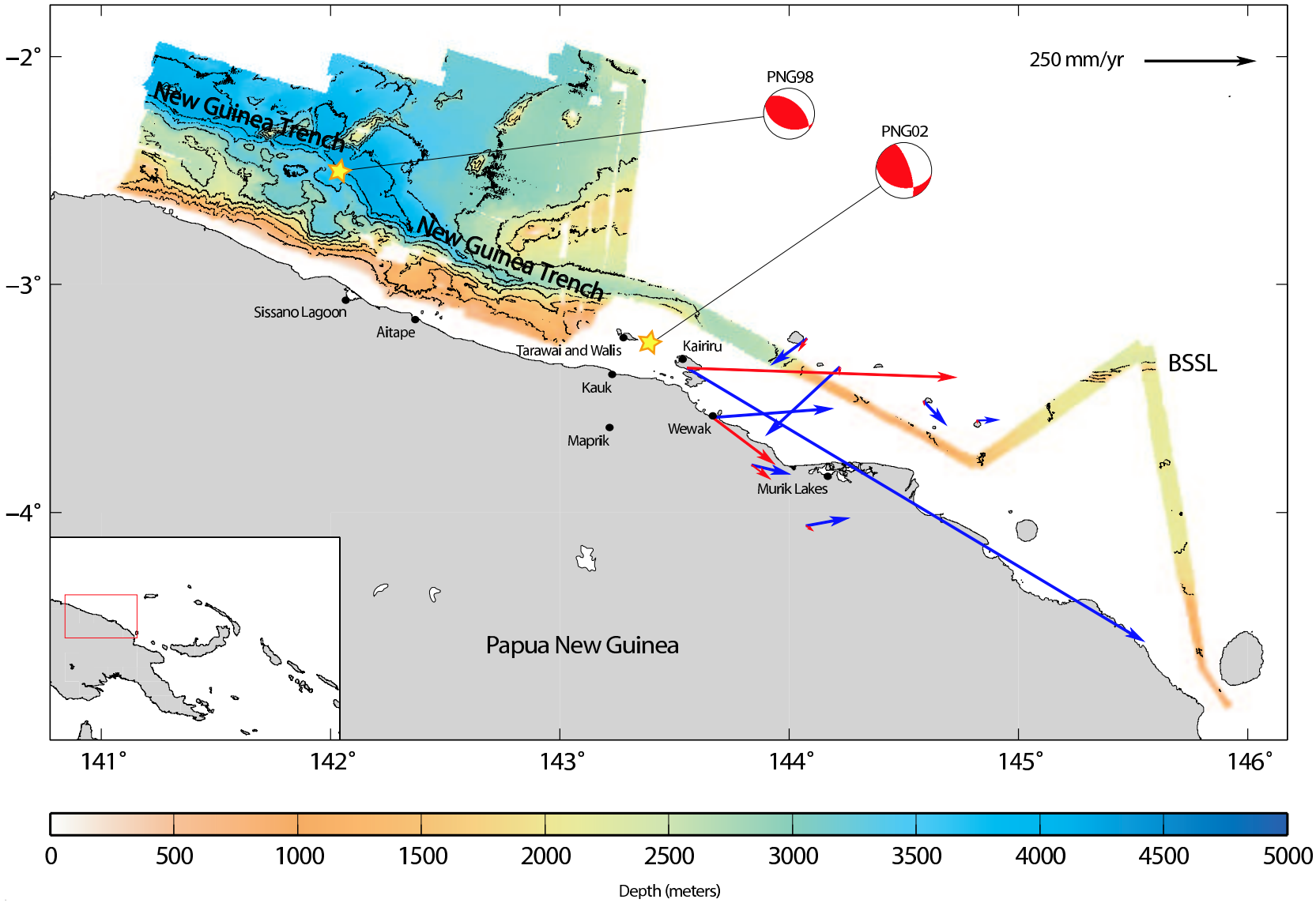


**Figure 1.1:** Map of the northern PNG coast showing bathymetry (D. Tappin, pers. comm. 2005) and tectonic boundaries. The Havard CMT focal mechansim is shown for the 1998 and 2002 events. Computed displacement vectors are shown for the 2002 event using the Harvard CMT focal mechanism (red). Also shown are the observed co-seismic displacments of this study (blue).

## 1.2 The 2002 $M_w$ = 7.6 Wewak Earthquake and Tsunami

The 2002 Wewak $M_w$ = 7.6 earthquake and tsunami occurred halfway between the villages of Aitape and Wewak near the intersection of the New Guinea Trench (NGT) and the Bismarck Sea Seismic Lineation (BSSL). The Preliminary Determination of Epicenters of the US Geological Society (PDE USGS) provide a hypocentral location of 3.30°S, 142.95°E. Focal mechanisms were provided for the event by the Harvard CMT ($\phi$ = 106°, $\delta$ = 34°, $\lambda$ = 43°) and USGS National Earthquake Information Center (NEIC) ($\phi$ = 80°, $\delta$ = 78°, $\lambda$ = 6°). The two focal mechanisms conflict, with the NEIC estimate showing a pure strike-slip geometry while the Harvard CMT estimate shows low angle thrust geometry. The Harvard CMT final solution was assumed by *Borrero et al.* (2003). The moment for the event is provided as $2.95 \times 10^{27}$ dyne-cm which, according to *Borrero et al.* (2003) using the scaling laws of *Geller* (1975), is consistent with a fault length = 72 km, width = 36 km, and slip = 2.1 m.

### 1.2.1 Earthquake Survey

The preliminary survey, established to assess the damage for governmental relief purposes, showed that, unlike the 1998 Sissano Lagoon event, it was the earthquake rather than the tsunami which caused most of the damage. Fortunately, only five people were killed by the event but as a result of building collapse and not the tsunami.

The majority of the damage was observed along the coastal regions and outer islands, but the earthquake was observed to have cracked water tanks as far inland as Maprik (30km from the coast) (*Davies*, 2002). The damage along the coast included cracked water tanks, subsidence of roads and the collapse of village dwellings made from local materials (*Davies*, 2002). In Wewak, a 20cm crack appeared in the runway of the airport and a water supply main was severed in two places (*Davies et al.*, 2002). Faults opened up nearly parallel to the coast, which is close to the assumed strike of the NGT. Liquefaction of unconsolidated subsurface sediments was common east of Kauk, and was most pronounced at Ubidnim where large blow-out holes caused water and sand to spout 3 - 5 m in the air (*Davies*, 2002). The liquefied sediments moved upwards filling open water wells, blocking fresh water for many villages (*Davies*, 2002).

On the outer islands, landslides were observed along the eastern and northern coasts of Kairiru, where fissures opened 10 - 30 cm (*Davies*, 2002). Uplift of 30 - 40 cm was observed

on the islands of Mushu, Kairiru, Tarawai and Walis. The most accurate record of this was from the south coast of Kairiru, where tide markings on a small pier indicated 35 cm of change (*Davies*, 2002). The uplift at Tarawai was observed by villagers to have occurred in two stages separated by one hour (*Davies*, 2002), indicating the fault may have ruptured in segments.

### 1.2.2 Tsunami Survey

Within 15 minutes of the main earthquake a tsunami was triggered that affected 300 km of the northern PNG coast between Sissano Lagoon and Murik Lakes. The run-up was generally less than 1.5 m but reached a maximum of 4 - 5 m in the western bays of the outer islands (*Davies et al.*, 2002).

The western extent of the tsunami was at Sissano Lagoon and Aitape, two sites that were devastated in the 1998 event. There, strong surges were observed into the lagoon and up the Aitape river. At nearby Mahol, residents feared a tsunami and fled inland. On return, they observed a line of pebbles on the beach recording the high water mark (*Davies et al.*, 2002). The central coast region between Kauk and Cape Moem was the hardest hit of the mainland sites with run-up of 2 m and inundation between 75 m and 190 m being observed (*Davies et al.*, 2002).

Flooding was observed on the offshore islands with a maximum run-up of 5 m in Victoria Bay and Mushu Bay. This large run-up is assumed to be the result of a funnelling effect; villagers observed the water to circulate around the bay in a counter clockwise direction (*Davies et al.*, 2002). On the islands of Walis and Tarawai villagers observed the sea to retreat, exposing reef 500 m offshore (*Borrero et al.*, 2003). The eastern most extent of the tsunami was observed at Murik Lakes where water flooded low lying coastal villages to ankle depth (*Davies*, 2002).

The overall effect of the tsunami was shown by *Borrero et al.* (2003) to be a moderate event, with a mechanism different from that of the 1998 Sissano Lagoon event. *Borrero et al.* (2003) used an *Okada* (1985) dislocation model to match the tsunami observations with the reef uplift and the Harvard CMT moment and focal mechanism.

## 1.3 Thesis aims and structure

The aim of this thesis is to:

- use GPS observations to estimate surface displacements resulting from the 2002 Wewak earthquake.
- describe a scenario that is consistent with these surface displacements and the published reef uplift and teleseismic data.
- develop a more advanced understanding of the tectonic setting along the northern coast of PNG.

This chapter has presented the problem and introduced the reader to some of the terminology which is to be used throughout this thesis.

*Chapter 2* provides a background to the tectonic and seismic setting along the northern PNG coast. This includes a description of the a priori plate model used in this study and a review of the region's major seismic events from the last century.

*Chapter 3* contains the analysis of GPS data collected along the northern PNG coast for the purpose of estimating site motions and co-seismic displacements.

In *chapter 4* I estimate the inter-seismic velocities for each GPS site. This includes my interpretation of the tectonic setting both prior to and after the earthquake.

In *chapter 5* I describe the methodologies used to invert the GPS observed co-seismic displacements to estimate earthquake fault parameters. This chapter concludes with the presentation of a model which best fits the observed GPS data and the previously published teleseismic and reef uplift data.

*Chapter 6* concludes the thesis with a summary of the results and a discussion on how this "best fitting" model enhances our present understanding of the tectonic situation along the northern PNG coast

# The Tectonic Setting

Papua New Guinea is situated in one of the world's most seismically active regions (*Pegler et al.*, 1995). A significant number of studies have used earthquake focal mechanisms (*Johnson and Molnar*, 1972; *Curtis*, 1973; *Pegler et al.*, 1995), Global Positioning System observations (*McClusky et al.*, 1994; *Tregoning et al.*, 1998; *Tregoning*, 2002; *Wallace et al.*, 2004), and geological mapping (*Davies et al.*, 1987) to show the complex array of active tectonic boundaries in the region. While these studies have been successful in identifying motions across many of the boundaries, very few have looked at the tectonics of the East Sepik coast.

The East Sepik Province is located along the northern coast of PNG between 143°E and 145°E. Within the last century at least eighteen significant[1] seismic events have occurred along this coast (*Everingham*, 1974); the two most recent being the devastating Sissano Lagoon ($M_w$ 7.1) earthquake and tsunami of July 17 1998 (PNG98)[2] and the Wewak ($M_w$ 7.6) earthquake and tsunami of 8 September 2002 (PNG02)[2]. Both earthquakes were felt throughout the East Sepik Province, with PNG98 resulting in many fatalities.

In this chapter I describe the geological and geophysical information regarding the past and present tectonic interpretation of the East Sepik region and provide reasoning for any constraints which have been placed on the assumed a priori plate configuration model. A review is also provided on the regions major seismic events from the last century.

[1] A significant event is assumed here to have a magnitude (M) greater than 7.0

[2] The terminology used by *Borrero et al.* (2003) will be used hereafter when referring to the 1998 and 2002 earthquakes.

## 2.1 Existing Models

PNG is situated between the Australian and Pacific Plates, where the dominant tectonic regime is one of convergence, with the Pacific Plate moving west-southwest at ∼110 mm/yr relative to the Australian Plate (*DeMets et al.*, 1994). Analysis of focal mechanisms, sea floor morphology and geodetic data have resulted in a number of different plate configuration models (*Johnson and Molnar*, 1972; *Curtis*, 1973; *Hamilton*, 1979; *Davies et al.*, 1987; *Tregoning et al.*, 1998; *Tregoning*, 2002; *Wallace et al.*, 2004) (Table 2.1). All of these studies agree with the existence of at least two minor plates; the South Bismarck (SBP) and the Solomon Sea (SS) Plates. The North Bismarck Plate (NBP) was first introduced by *Johnson and Molnar* (1972) and is situated to the north of the SBP, separated by the Bismarck Sea Seismic Lineation (BSSL). *Hamilton* (1979) and *Davies et al.* (1987) proposed a Woodlark Plate, located in the Woodlark Basin of the Solomon Sea. Further speculation has also been made to the existence of the Caroline (*Weissel and Anderson*, 1978), Trobriand (*Davies et al.*, 1984), Highlands and Adelbert (*Wallace et al.*, 2004) Plates.

The most recent study into PNG's active tectonics is by *Wallace et al.* (2004), whose model uses GPS velocities and earthquake slip vectors to describe the existence of six plates; the Australian, Pacific, South Bismarck, North Bismarck, Woodlark and the previously unrecognised New Guinea Highlands Plate (Figure 2.1).

### 2.1.1 Bismarck Sea Seismic Lineation

The SBP was first proposed by the focal mechanisms of *Johnson and Molnar* (1972). The plate is defined by *Taylor* (1979) to occupy most of the South Bismarck Sea, New Britain Island Arc, Huon Peninsula, and stretch as far west as Madang. In the south the New Britain Trench accommodates the subduction of the Solomon Sea Plate (*Tregoning et al.*, 1998), while the seismically active Weitin Fault defines the eastern bound (*Taylor*, 1979). The northern boundary is with the NBP and is defined by a narrow band of seismicity, referred to as the Bismarck Sea Seismic Lineation. The boundary stretches from the northeastern tip of New Britain in the east to the northern coast of New Guinea in the west. *Tregoning* (2002) shows that west of 146.5°E the BSSL runs east - west with a relative motion between the SBP and the NBP of ∼116 mm/yr along-strike and ∼30 mm/yr down-dip (Table 2.2).

**Table 2.1:** Proposed plate configuration models from the literature. SBP = South Bismarck, SS = Solomon Sea, NBP = North Bismarck, WLK = Woodlark, TBD = Trobriand, MAN = Manus, ADL = Adelbert and NGH = New Guinea Highlands.

| | Plates | | | | | | | |
|---|---|---|---|---|---|---|---|---|
| Study | SBP | SS | NBP | WLK | TBD | MAN | ADL | NGH |
| Johnson and Molnar (1972) | ○ | ○ | ○ | | | | | |
| Curtis (1973) | ○ | ○ | | | | ○ | | |
| Hamilton (1979) | ○ | ○ | | ○ | | | | |
| Davies et al (1984) | | ○ | | ○ | ○ | | | |
| Tregoning et al (1998) | ○ | | | ○ | | | | |
| Tregoning et al (1999) | ○ | | | ○ | | | | |
| Tregoning (2002) | ○ | | ○ | ○ | | | | |
| Wallace et al (2004) | ○ | | ○ | ○ | | | ○ | ○ |

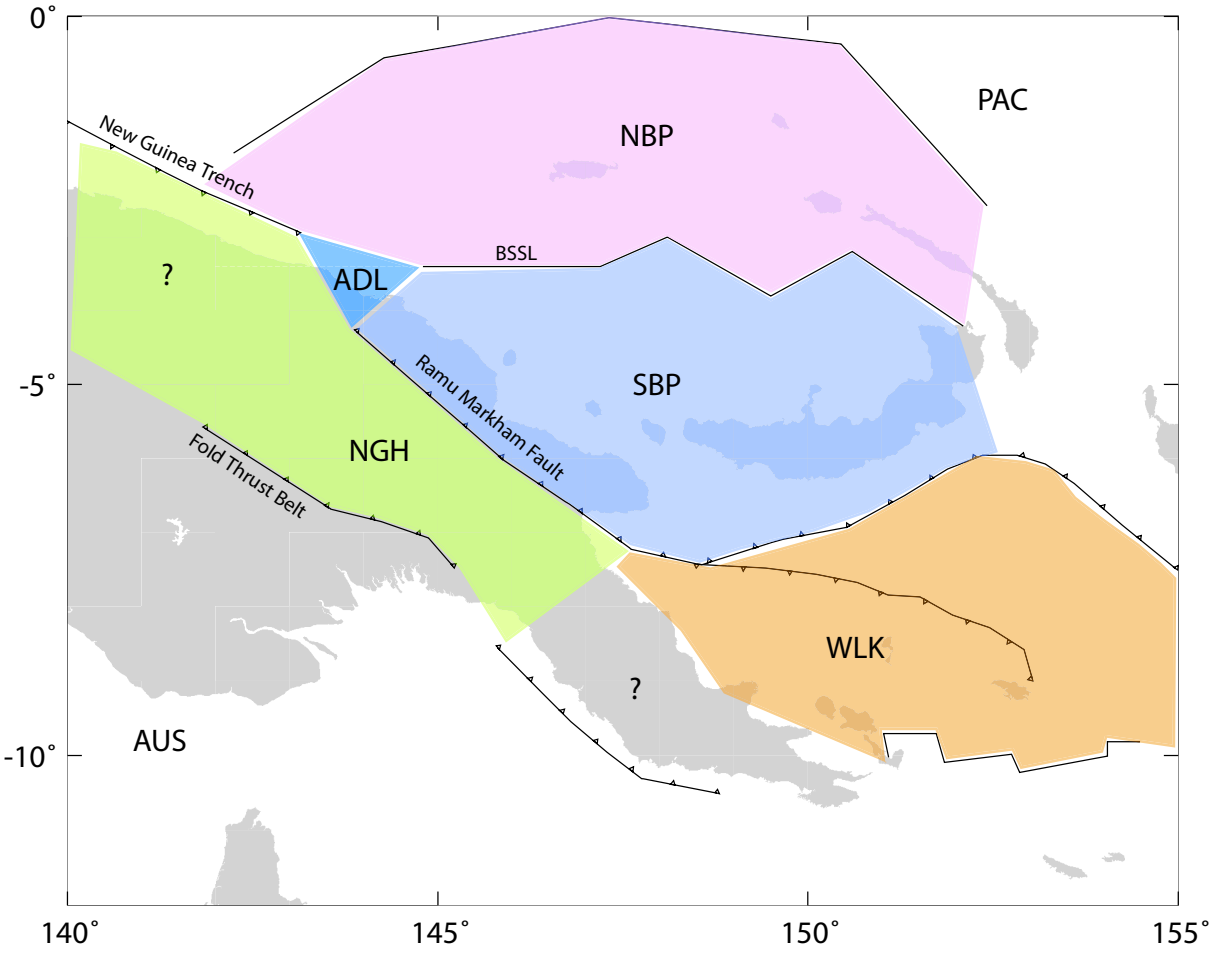


**Figure 2.1:** Tectonic block configuration in PNG (*Wallace et al.*, 2004). AUS = Australian, PAC = Pacific, NBP = North Bismarck, SBP = South Bismarck, WLK = Woodlark, NGH = New Guinea Highlands, ADL = Adelbert and BSSL = Bismarck Sea Seismic Lineation.

*Cooper and Taylor* (1987) show a narrow band of shallow earthquakes running inland across the northern New Guinea region. From this evidence some authors have postulated the theory that the BSSL continues westward across New Guinea where it meets the Sorong Fault in northern Irian Jaya (eg. *Klootwijk et al.*, 2003). *Hamilton* (1979) and *Johnson* (1987) show an alternate theory that, prior to crossing the northern New Guinea coast, the BSSL merges with the New Guinea Trench in a trench - fault junction. A limited track of bathymetry data situated between 144°E and 145.5°E shows a ridge which is indicative of the BSSL running in an east - west direction at 3.40°S (D. Tappin, pers. comm. 2005). If the BSSL did continue westward it would cross the coast between the village of Wewak and the islands Kairiru and Mushu (Figure 2.2).

### 2.1.2 Southern Boundary of the South Bismarck Plate

The south-western boundary of the SBP is described by *Johnson and Molnar* (1972) as being a continent-island arc collision across the Ramu-Markham Fault (RMF). The RMF is a shallow north-east dipping (15°) mid-crustal detachment that joins a steeply dipping (40°) ramp at a depth of about 20km (*Pegler et al.*, 1995; *Stevens et al.*, 1998). *Johnson and Molnar* (1972) describe the RMF to be the boundary between the rigid Australian and the SBP. *Wallace et al.* (2004) propose the existence of a New Guinea Highlands (NGH) Plate here in place of the Australian Plate.

The proposed NGH Plate is based on GPS velocities estimated across the eastern edge of the New Guinea Highlands. The extents of this plate are indicated to be the New Guinea Highlands Fold and Thrust Belt to the south, the RMF in the north and the Woodlark Plate to the east. The western extent is not defined, but could extend across New Guinea into Irian Jaya (*Wallace et al.*, 2004) (Figure 2.1).

*Pegler et al.* (1995) identified from earthquake relocations an inverted U-shaped zone of seismicity situated at intermediate depth beneath the Finisterre and New Guinea Highlands, which was inferred to be a doubly subducted slab of the Solomon Sea Plate lithosphere. This slab is assumed by *Tregoning and Gorbatov* (2004) to lie below the subducting NBP slab at the NGT, indicating that deep seismicity observed in this region may be from the subducted SS Plate rather than at the NGT.

*Tregoning et al.* (1999) describe the north-western boundary of the SBP to be a gentle transition, due to low strain rates and the absence of substantial seismic activity. The relative

pole of rotation between the SBP and the Australian Plates is situated in this region (Table 2.2), hence velocity estimates are similar for both plates. *Wallace et al.* (2004) describe a shallow trend of strike-slip events east of this boundary and suggest the possible existence of the Adelbert Block, but leave it out of their model due to inconclusive evidence.

### 2.1.3 New Guinea Trench

*Okal* (1999) relocated over 220 historical and recent earthquakes, including the 1996 $M_w$ = 8.2 Biak event, to show that there is evidence of seismic activity across the New Guinea Trench west of 138°E. Before the Biak event many authors (eg. *Everingham*, 1974; *Puntodewo et al.*, 1994) had commented on a lack of seismic activity across the NGT, with *Okal and Cazenave* (1985) suggesting the NGT may be a waning subduction zone. These comments were supported by early tomographic imagery that showed no evidence of active subduction across the NGT (*Okal*, 1999; *Gutscher et al.*, 2000). *Tregoning and Gorbatov* (2004) concluded from recent tomographic imagery that there is clear evidence of active southwestward subduction along the entire NGT. This observation supports the conclusions made by *Okal* (1999) and is consistent with the occurrence of recent large thrust events across the fault (eg. Biak, PNG98 and PNG02).

East of 141°E, bathymetric data clearly identifies the NGT running SE at ∼112°to the eastern extent of the data at 143.5°E (*Tappin et al.*, 2001). West of 143.5°E, aftershocks from PNG02, located by the PDE, show the approximate extension of the NGT to ∼3.5°S, 144.0°E. *Tregoning and Gorbatov* (2004) show the dip angle of the trench to range from 30°at 136°E to 10°at 143°E. *Hurukawa et al.* (2003) used a method of joint hypocenter de-

**Table 2.2:** Absolute and Relative Angular Velocity Vectors for the Australian, North Bismarck, South Bismarck and New Guinea Highlands Plates. In all cases the Euler vectors are for the second plate with respect to first. $e_{max}$, $e_{min}$ and azimuth refer to the maximum and minimum uncertainties of the error ellipse and the azimuth of the major axis. Estimates are from *Wallace et al.* (2004) and **Tregoning* (2002).

| Plate Pairs | Latitude | Longitude | Rate °/Myr | $e_{max}$ | $e_{min}$ | Azimuth |
|---|---|---|---|---|---|---|
| ITRF00-AUS | 32.00 | 39.13 | $0.621 \pm 0.003$ | 0.59 | 0.33 | 163 |
| ITRF00-NGH | -7.56 | 145.98 | 1.63 | - | - | - |
| | | | | | | |
| AUS-SBP | -4.18 | 144.02 | $-7.45 \pm 0.13$ | 0.14 | 0.05 | -18 |
| AUS-SBP* | -4.36 | 144.54 | $-7.91 \pm 0.33$ | 0.24 | 0.16 | 281 |
| AUS-NBP | -51.3 | 165.31 | $1.25 \pm 0.06$ | 4.71 | 0.35 | 113 |
| AUS-NBP* | -50.6 | 166.7 | $1.23 \pm 0.07$ | 4.1 | 0.4 | 37 |
| AUS-NGH | -7.56 | 145.98 | $1.63 \pm 0.20$ | 0.36 | 0.18 | 148 |

termination to relocate PNG98 and its aftershocks and delineate a dip angle of 19°. The estimates of dip from *Tregoning and Gorbatov* (2004) and *Hurukawa et al.* (2003) are consistent with the early observations of *Denham* (1969) who suggests a trench that "dips gently to the south."

South of the NGT, GPS velocities are shown at Wewak (WEWK), Vanimo (VANI) (*Tregoning et al.*, 2000), and Jayapura (ANGS (*Kato et al.*, 1998) and SENT (*Bock et al.*, 2003)) to be 30% slower with a 10°counter-clockwise rotation than the well estimated rigid Australian Plate. *Tregoning et al.* (2000) suggests that this region may either be moving as a separate tectonic block or being influenced by inter-seismic strain accumulation, but their interpretation was limited due to insufficient geodetic data.

### 2.1.4 A Priori Plate Model

From the available geophysical information it appears that the East Sepik region accommodates the movement of at least three tectonic blocks; NBP, SBP and NGH. Inconclusive GPS observations (*Kato et al.*, 1998; *Tregoning et al.*, 2000; *Bock et al.*, 2003) indicate that the Sepik region may not be moving as part of the Australian rigid plate, further suggestion has indicated that this region may be moving as part of a NGH Plate. To avoid unnecessary speculation, I will in this study refer to the region as Block "A", which may contain tectonic signals from both the Australian and NGH Plates.

Active subduction of the NBP is occurring across the New Guinea Trench at ∼108 mm/yr S71°W[3]. The BSSL is accommodating left-lateral strike slip movement between the SBP and NBP of ∼116 mm/yr with ∼30 mm/yr of convergence. The NGT runs at a strike of ∼112°to approximately 3.4°S, 144.0°E, where it meets the east - west trending BSSL, which continues westward across New Guinea. Figure 2.2 shows the a priori plate model as described above.

## 2.2 Seismicity of the East Sepik

Earthquakes regularly occur along the northern PNG coast, many of which are tsumagenic (*Everingham*, 1974). A number of studies have relocated earthquakes within this region to help constrain fault location and geometry (*Denham*, 1969; *Johnson and Molnar*,

[3]This is stated assuming Block "A" is moving with the Australian Plate

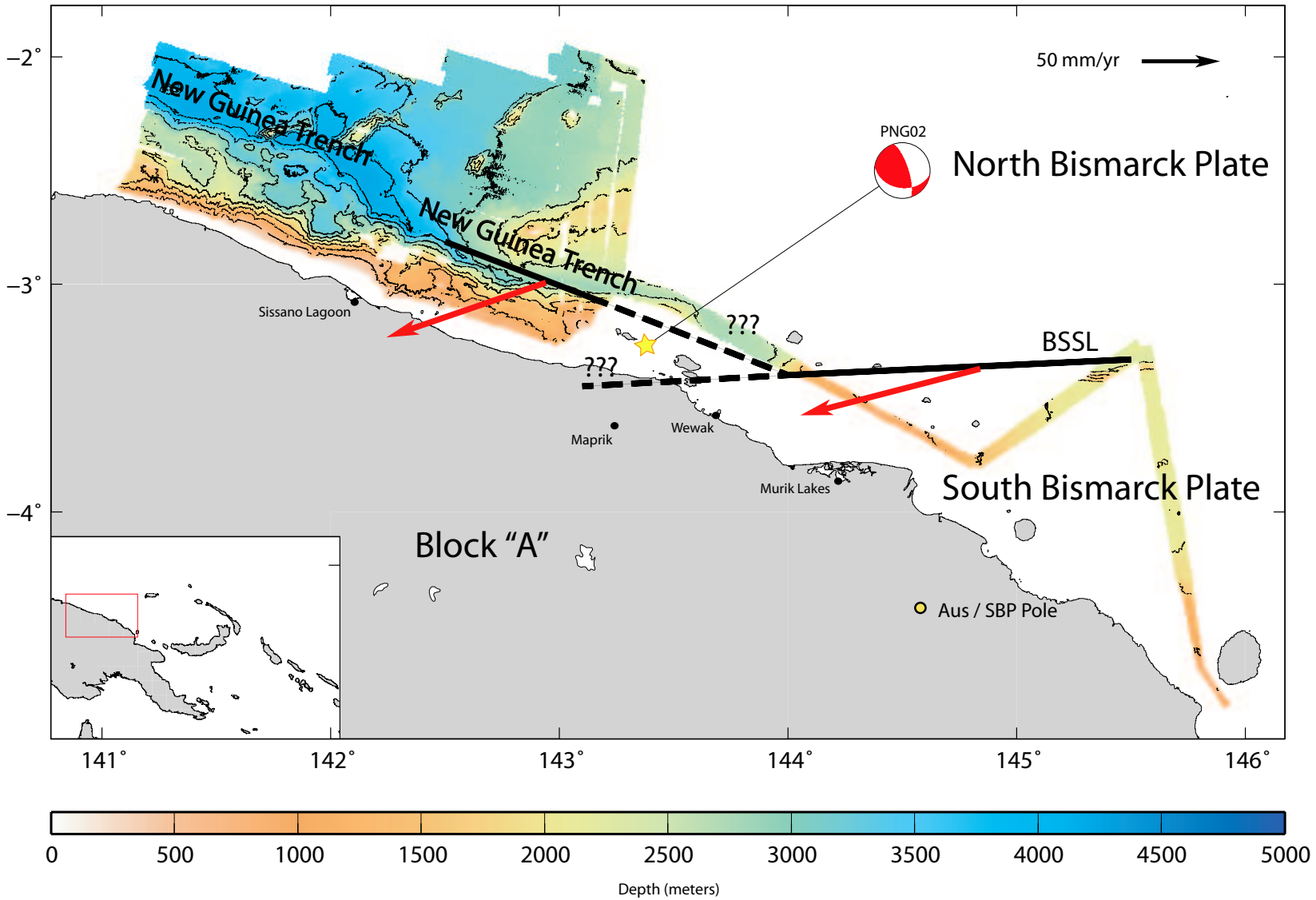


**Figure 2.2:** A priori plate configuration model for the East Sepik region used in this study. Shown is bathymetric data (D. Tappin, pers. comm. 2005), North Bismarck Plate relative velocities (red) and Australian - South Bismarck Euler Pole (*Tregoning et al.*, 1999). Also shown is the Harvard CMT focal mechanism for PNG02.

1972; *Hamilton*, 1979; *Pegler et al.*, 1995). During the last century there have been eighteen seismic events with M $>$ 7 in the East Sepik Province. In 1918 and 1968 two shallow M $\approx$ 7 events occurred at the NGT near the location of PNG02, from this I infer that this part of the NGT has a seismic repeat period of $\sim$50 years.

### 2.2.1 Seismic Events

Figure 2.3a provides the locations and where available the Harvard CMT focal mechanisms of the most significant events of the last century from the East Sepik coast. Figure 2.3b shows the Harvard CMT focal mechanisms for PNG02 and associated aftershocks.

- On 15 December 1907, a slow subsidence M = 7.4 event relocated at 3.1°S, 142.5°E doubled the size of Sissano Lagoon (*Everingham*, 1974).
- On 3 July 1918, a shallow M = 7.2 event occurred inland from the coast at 3.47°S, 143.22°E (USGS)[4]
- A $M_w$ 7.9 event on 20 September 1935 occurred inland (3.5°S, 141.8°E) at a depth greater than 50km hence causing little devastation (*Borrero et al.*, 2003).
- On the 22 February 1951, a small tsunami was triggered near the village of Aitape and was relocated at 3.30°S, 142.17°E (*Borrero et al.*, 2003).
- On 23 October 1968, a M = 7.1 event occurred in the New Guinea Trench near the location of PNG02 at 3.37°S, 143.32°E (USGS)[4].

On 17 July 1998, one of PNG's worst natural disasters occurred when an $M_w$ 7.1 earthquake triggered a tsunami with maximum wave height of 15m near Sissano Lagoon (*Hurukawa et al.*, 2003). As a result of the tsunami, many coastal villages were destroyed and a death toll exceeding 2000 people was recorded. Many studies have presented details on the submarine slump which caused the tsunami (*McSaveney et al.*, 2000; *Tappin et al.*, 2001; *Davies et al.*, 2003; *Satake and Tanioka*, 2003), relocated the focal plane as an inter-plate event (*Hurukawa et al.*, 2003) and provided what is probably the most in-depth discussion on seismicity and tectonics along the northern PNG coast.

The most recent large event surrounding the East Sepik coast was the 2002 Wewak earthquake and tsunami (PNG02), which is the main focus for this thesis.

[4]US Geological Survey (2002), Papua New Guinea Earthquake of 8 September 2002, near the location of PNG02, Historic Earthquakes Poster, (http://neic.usgs.gov).

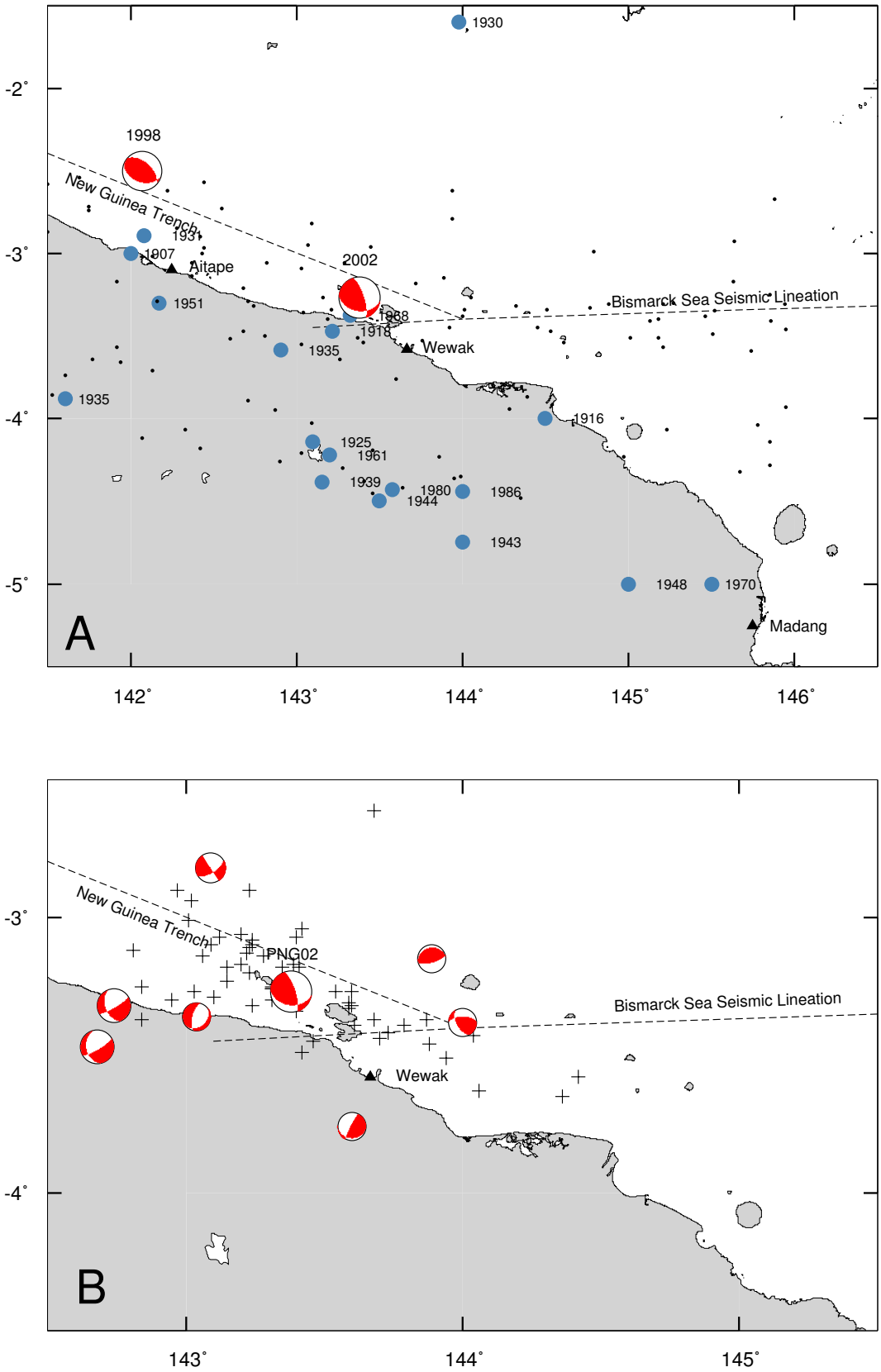


**Figure 2.3:** (a) Map of historical seismic events from the East Sepik coast. Events with M > 7.0 are shown in blue, all other events are shown in black. Also shown are the Harvard CMT focal mechanisms for PNG98 and PNG02. (b) Location map of PNG02. Harvard CMT focal mechanisms are shown for significant after shocks (red). Also shown are PDE USGS locations of all aftershocks (black crosses).

# Geodetic Analysis

Over the past decade, GPS has become a common tool for monitoring plate kinematics and surface deformation. During this time the reliability and repeatability of GPS analysis has increased dramatically, primarily due to the increasing size of the satellite constellation, advancements in receiver technology and improved processing methodologies. Given that there is now such a widespread use of GPS, this chapter will focus only on the methodology I used to process data for this study. Further discussion on GPS technology and processing methodologies can be found in the literature (see *Dixon*, 1991; *Feigl et al.*, 1993; *Rizos*, 1996; *Dong et al.*, 1998).

## 3.1 GPS Data Set

GPS observations have been made in the PNG region by the Australian National University (ANU), the University of Canberra, the University of Papua New Guinea and the National Mapping Bureau of Papua New Guinea, since 1990 (*McClusky et al.*, 1994; *Tregoning et al.*, 1998). In 2000, the ANU established an 8 site GPS network spanning the BSSL and NGT to monitor the build up of elastic strain (Figure 3.1). Prior to the second set of observations being made at XAVI, BAMI, MUTM, TARO and KOIL, the PNG02 earthquake occurred, displacing all sites. Immediately after the event observations were made at WEWK, XAVI, TARO, KOIL and TRNG. The sites BAMI, MUTM and ANGR were not re-observed for over a year after PNG02. Observations have since continued for all sites at approximately yearly intervals; hence the data set now contains sufficient observations to make valid estimates of surface displacement from PNG02.

Data from two nearby sites Maprik (MPRK) and Ambunti (ABTI) have been included in the network to assist in the interpretation of the regions inter-seismic setting. These sites were not observed before PNG02. Table 3.1 shows the GPS data analysed in this study.

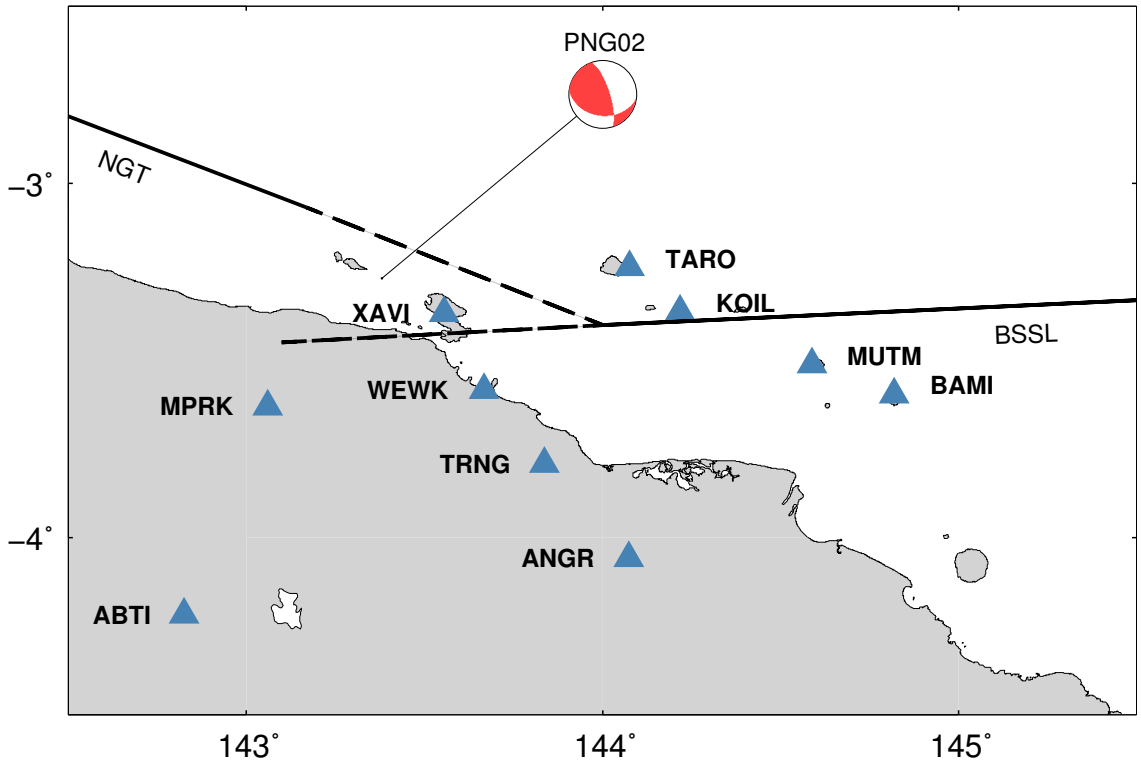


**Figure 3.1:** Locations of the GPS sites used in this study. The Harvard CMT focal mechanism is plotted for PNG02, the dashed lines are assumed a priori locations of the BSSL and NGT.

## 3.2 GPS Data Analysis

I analysed the GPS observations using a regional network procedure. Site coordinates were estimated in 24 hours blocks (each block corresponding to a UTC day), and constrained to the International Terrestrial Reference Frame (ITRF) by a regional network of dedicated International GNSS Service (IGS) sites. The processing was performed using GAMIT (*King and Bock*, 2000) and the GLOBK Kalman filter program (*Herring*, 1999). The following provides a brief overview of the software and how it was used.

### 3.2.1 Daily Solutions

GAMIT is a series of programs developed to analyse GPS phase data and estimate a loosely constrained set of parameters (*King and Bock*, 2000). The parameters estimated are site coordinates, satellite orbital parameters, tropospheric delay parameters, phase ambiguities, and Earth orientation parameters. IGS satellite orbits were used as a priori information from which regional orbits were estimated. The regional orbital model consists of 15 parameters per satellite (an X, Y, Z cartesian coordinate, 3 velocities, and 9 force model parameters as described by *Beutler et al.* (1994)).

**Table 3.1**: Observation Periods for GPS Sites used in this Study

| Sites | Code | Long. | Lat. | 1993 | 1997 | 1999 | 2000 | 2002 | 2003 | 2004 | 2005 |
|---|---|---|---|---|---|---|---|---|---|---|---|
| Ambunti | ABTI | 142.852 | -4.218 | | | | | | 305-309 | | 192-195 |
| Angoram | ANGR | 144.073 | -4.057 | | | | 198-202 | 115-118 | 299-301 | | |
| Bam Bam | BAMI | 144.819 | -3.597 | | | | 257-263 | | 321-324 | 330-335 | |
| Koil | KOIL | 144.218 | -3.362 | | | | 258-259, 262-263 | 258-262 | 320-324 | 330-335 | |
| Maprik | MPRK | 143.059 | -3.361 | | | | | | 304-307 | | 192-195 |
| Mut Mut | MUTM | 144.587 | -3.512 | | | | 256-259 | | 320-324 | 330-335 | |
| Taro | TARO | 144.076 | -3.238 | | | | 258-263 | 258-262 | 320-324 | 330-335 | |
| Tring | TRNG | 143.836 | -3.792 | | | | 199-203 | 115-118, 261-262 | | | |
| Wewak | WEWK | 143.666 | -3.584 | 231-232, 234-237 | 122, 244-250 | 064-066 | 194-198 | 116-117, 257-260 | | | 191-196 |
| Kairiru | XAVI | 143.554 | -3.367 | | | | 258-263 | 258-262 | 320-324 | 330-335 | 197-201 |

A number of different routines and options can be applied during processing to enhance the solution. Prior to processing, it is important for the data to be "cleaned", this includes the removal of cycle slips and obvious outliers. The AUTCLN routine is used to remove cycle slips and to reduce phase ambiguities to integer values.

In this study I used GAMIT to process carrier phase observations from the local PNG network between the years 2000 and 2005 (with the exception of WEWK where observations began in 1993). Included with these local sites were 24 regional IGS sites. The reason for incorporating regional IGS sites into the solution is to constrain the fiducial-free network to the ITRF, in which each IGS site has reliable coordinates (*Beutler et al.*, 1999). As the processing was performed in a regional network, I solved for all carrier phase ambiguities and minimised the ionospheric effect by using a linear combination of the two GPS signal frequencies (*Rizos*, 1996). The resulting solutions from GAMIT are variance-covariance matrices and estimated parameters for each UTC day. The matrices are provided as input to the GLOBK program.

### 3.2.2 Estimation of ITRF2000 Site Coordinates

GLOBK is a Kalman filter program which is used to combine various different types of geodetic data to produce estimates of site velocities, satellite orbits and Earth orientation parameters (*Herring*, 1999). An advantage of a Kalman filter is that it can be used to align loosely constrained solutions with those of a defined reference frame (*Tregoning et al.*, 1998). It is this feature that I have used in this study.

As part of the GAMIT solution I included 24 regionally located IGS sites, all of which have coordinates in the ITRF2000 that have been independently verified using other space geodetic techniques, such as Very Long Baseline Interferometry (VLBI) (*Beutler et al.*, 1999). 10 of these 24 IGS sites were adopted as fiducial sites (Figure 3.2).

I used GLOBK to align each daily GAMIT solution to the ITRF2000 by providing a best fitting adjustment based on tightly constraining the horizontal coordinates of the 10 stable IGS sites to 0.005 m. Outliers[1] were removed from the time series, leaving a set of coordinates in the ITRF2000 for each site for each day.

[1] a point which did not fit its neighbouring point at the $3\sigma$ level or 99.7% confidence interval was deemed an outlier.

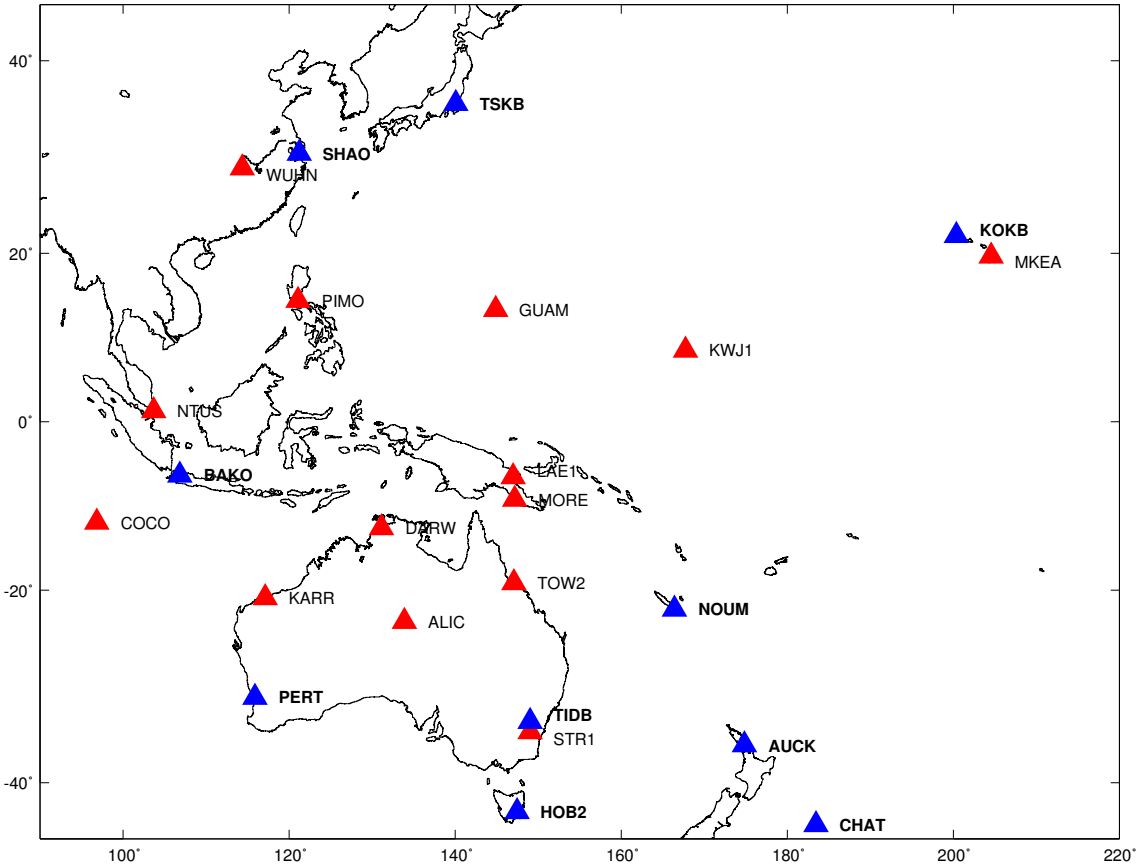


**Figure 3.2:** Regional IGS sites used in the GPS processing to strengthen the solution and estimate coordinates with reference to the ITRF2000. The blue triangles represent sites that were tightly constrained to their ITRF2000 values.

## 3.3 Time Series and Accuracy

GPS position estimates are influenced by a number of tectonic signals (eg. co- and post-seismic motion). These signals appear in the time series as discontinuities and non-linear trends (Figure 3.3). The main tectonic signal which can be seen in the time series from this study is a discontinuity in mid September 2002 (Figure 3.4); assumed to be co-seismic displacement from PNG02. To estimate the magnitude of the displacement a reliable estimate of the inter-seismic velocity both before and after the earthquake is required. The minimum requirement for a velocity estimate is two position estimates; but three position estimates will provide redundancy. With the exception of WEWK, none of the GPS sites observed have multiple observations both before and after PNG02, only three sites have velocity estimates before (WEWK, ANGR and TRNG), and only four sites have redundant observations (WEWK, XAVI, KOIL and TARO).

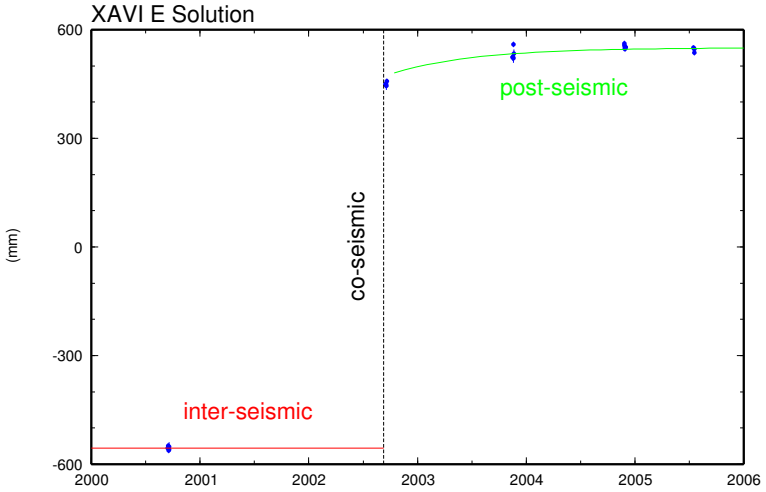


**Figure 3.3:** Times series for XAVI (east component). Co-seismic displacement is evident for PNG02. Post-seismic relaxation is also indicated after the event.

To estimate the inter-seismic velocities at the sites I fitted a linear regression function to the data from either before (ANGR, TRNG and WEWK) or after (TARO, KOIL, BAMI, MUTM, XAVI, WEWK, MPRK and ABTI) PNG02, dependent on when multiple observations were made. Analysis of the resulting velocity estimates revealed that the sites which have multiple occupations after PNG02 show non-linear motion, as the observed site positions do not fit a regression line (eg. Figure 3.3). The velocity estimates were made taking only the co-seismic signals from PNG02 into account; hence it is likely that the non-linear motion is the result of an un-modelled co- or post-seismic signal after PNG02.

At XAVI, a clear non-linear trend is seen in the east component for observations made after PNG02. The linear trend estimated for the data after the earthquake is shown to be 34 mm/yr. The observations do not fit this line and show motion which is beginning to trend west, hence it is clear that XAVI does not display linear motion after PNG02. To test whether the site is undergoing post-seismic relaxation I fitted an exponential curve of the type shown by equation 3.1 to the observations. Post-seismic signals are shown by *Savage and Svarc* (1997) to display exponential characteristics such as natural decay rates. The exponential curve applied provides a good estimate of the observed motion (Figure 3.4).

$$y = a_1 + a_2 \times e^{\frac{-\tau}{a_3}} \tag{3.1}$$

**Table 3.2:** Multiple velocity estimates made at TARO and KOIL (a) using all observations after PNG02 (b) using observations between 2002 - 2003 and (c) using observations between 2003 -2004. Velocities are in mm/yr.

| Site | Component | All | 02 - 03 | 03 -04 |
|---|---|---|---|---|
| TARO | E | -86 | -104 | -66 |
| | N | 15 | 5 | 27 |
| KOIL | E | -54 | -54 | -55 |
| | N | 15 | 5 | 20 |

Two sets of observations have been made at WEWK since the earthquake; therefore there is insufficient data to demonstrate that post-seismic relaxation is occurring. However, the linear velocity estimated from data after the earthquake is 42 mm/yr greater than the well resolved inter-seismic velocity of 12 mm/yr derived from five occupations before PNG02. Overlaying an exponential curve to the observations after PNG02 (with the same time constant as the curve fitted to XAVI) matches the observations, and the curve turns asymptotic at a velocity similar to the well determined inter-seismic velocity from before PNG02. This is an indication that WEWK is also undergoing post-seismic relaxation.

The sites KOIL and TARO both have three sets of observations made after PNG02, hence multiple velocity estimates can be made to check the accuracy of the linear velocity estimate. Table 3.2 shows the sites do not display linear motion after PNG02 (with the exception of the east component of KOIL). As the velocity estimates at XAVI and WEWK both indicate the possibility of post-seismic relaxation occurring it would be a reasonable assumption that both KOIL and TARO, which are closer to the NGT, could also be undergoing a similar relaxation. Further discussion on the observed non-linear motion at KOIL and TARO is continued in section 4.2.1 and the effect of post-seismic relaxation is continued in section 5.1.1.

The remaining sites (BAMI, MUTM, ANGR, TRNG, ABTI and MPRK) have velocity estimates that have been derived between two sets of observations, hence it is not possible to show if non-linear motion is present. Care is therefore taken when interpreting the velocities. In figure 3.4 the uncertainty given to each velocity estimate is based on the formal uncertainty of the estimated site positions. For sites which have only a single occupation either before or after PNG02, the velocity has been assumed to be the same as the velocity calculated on the opposing side.

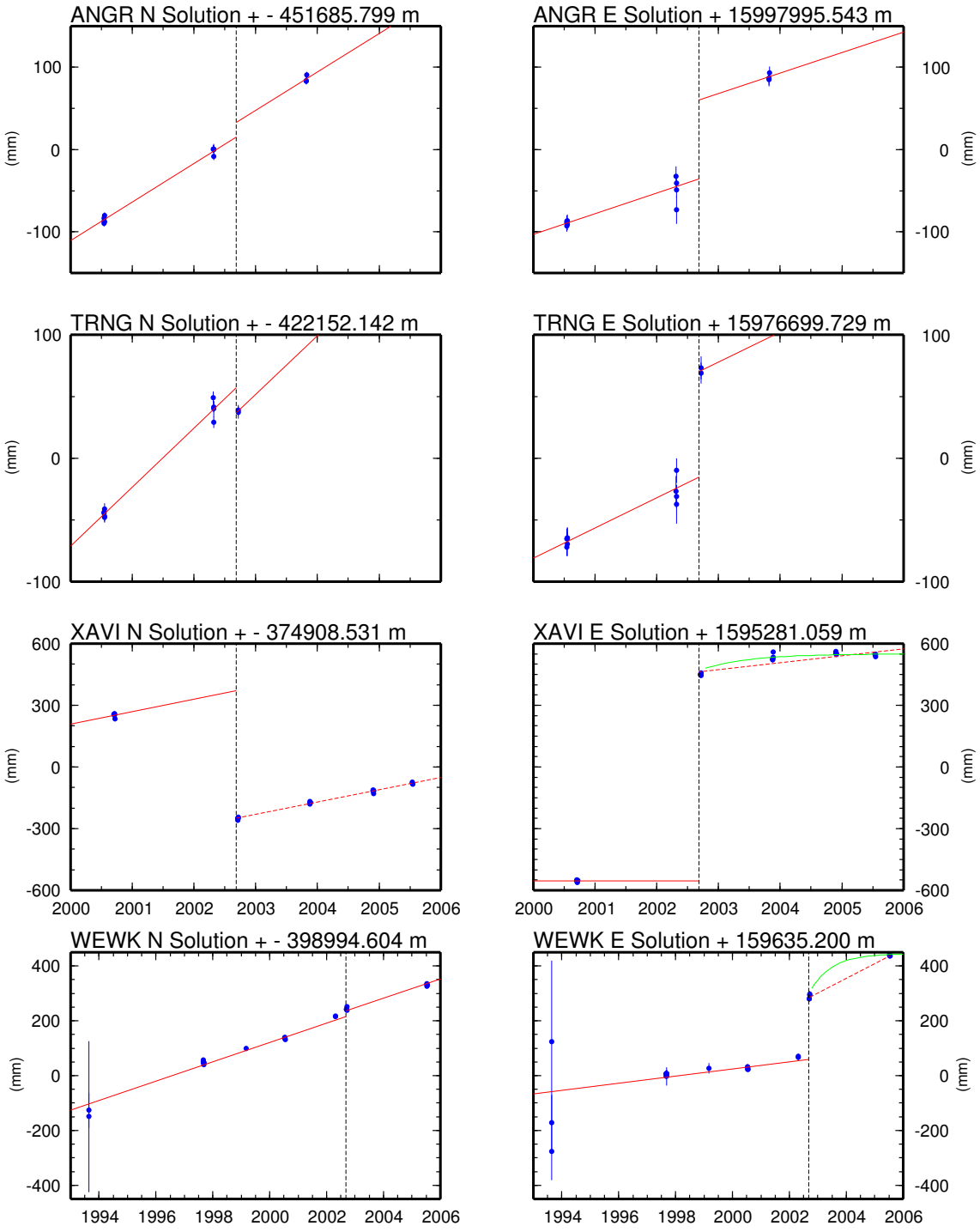


**Figure 3.4:** The position estimates in the ITRF2000 coordinate system. The estimated inter-seismic velocity at each site is represented by the slope of the regression line (red). PNG02 is shown as a vertical dashed line (black). The velocity at WEWK and XAVI is shown in (red) and overlaid with a best fitting exponential curve (green). Also velocities at KOIL and TARO are represented by dashed lines (red) as their linear fit is questioned in section 4.2.1.

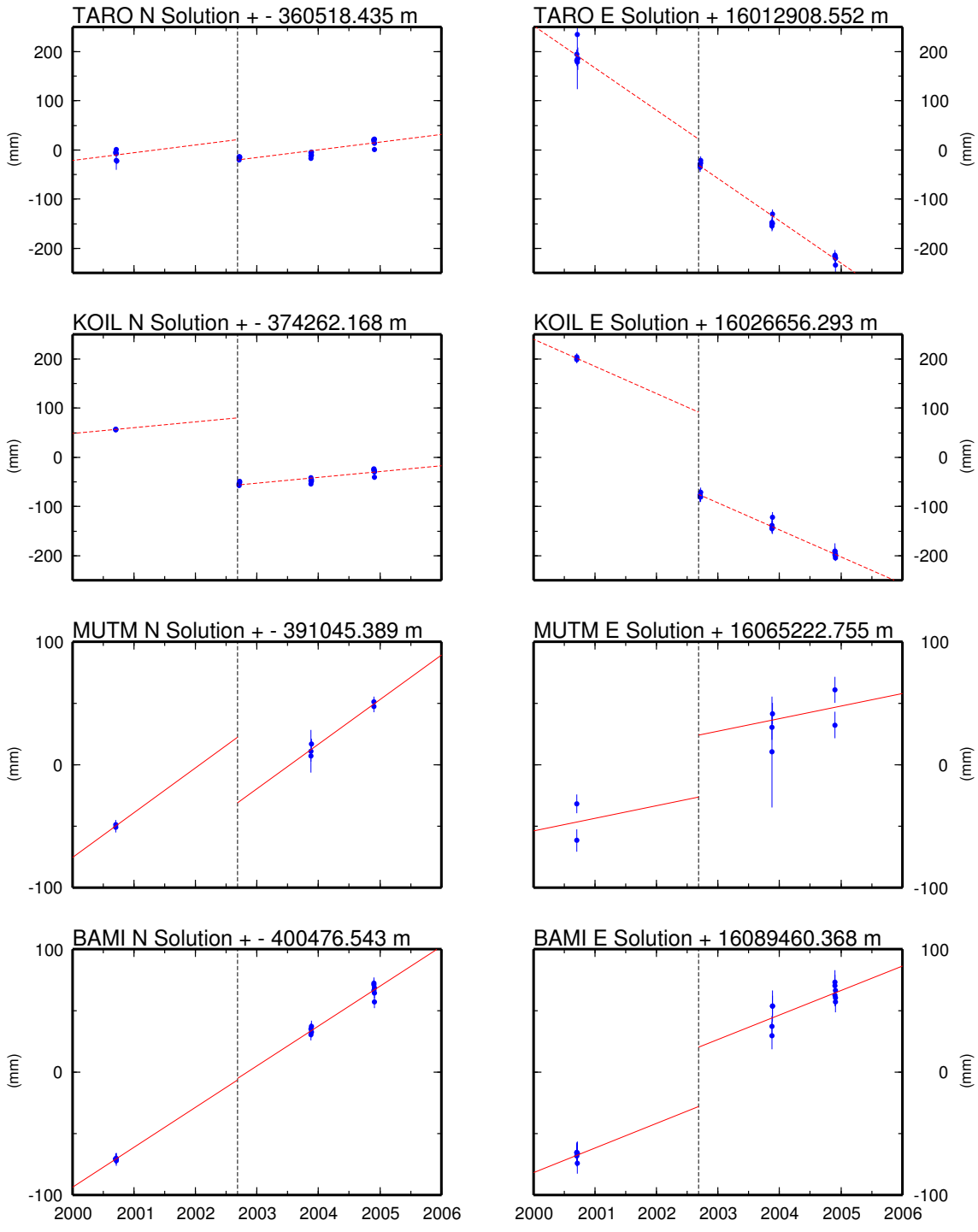
TARO N Solution + - 360518.435 m
TARO E Solution + 16012908.552 m
KOIL N Solution + - 374262.168 m
KOIL E Solution + 16026656.293 m
MUTM N Solution + - 391045.389 m
MUTM E Solution + 16065222.755 m
BAMI N Solution + - 400476.543 m
BAMI E Solution + 16089460.368 m
(mm)
2000
2001
2002
2003
2004
2005
2006

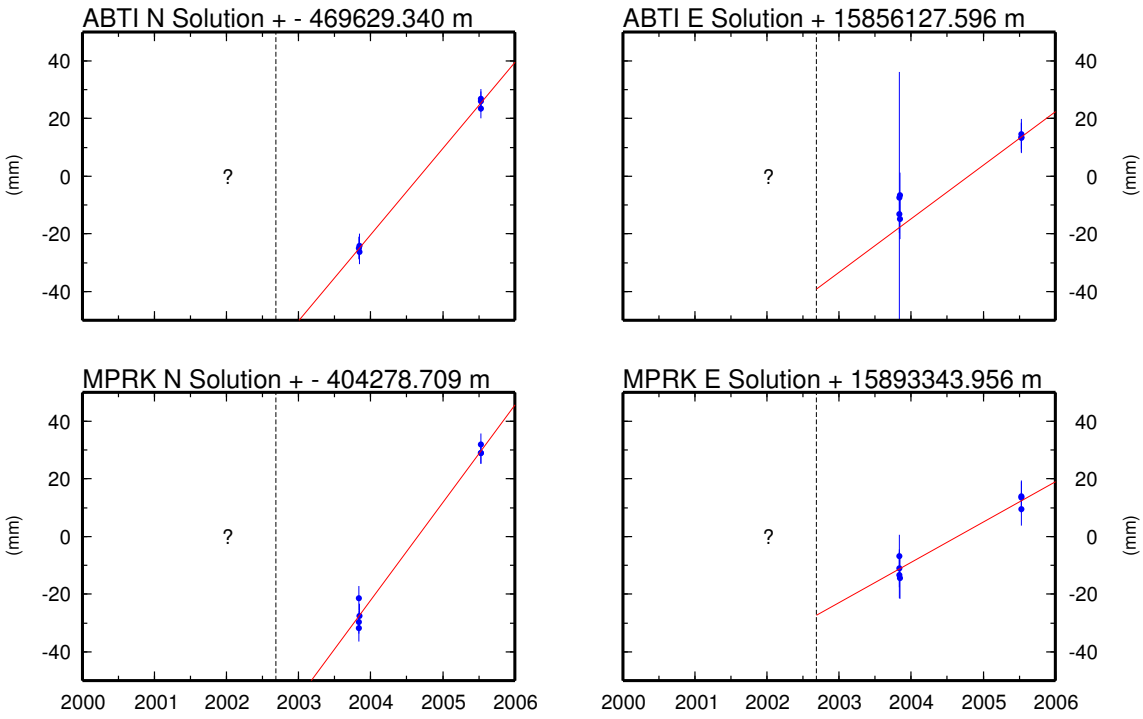
ABTI N Solution + - 469629.340 m
ABTI E Solution + 15856127.596 m
MPRK N Solution + - 404278.709 m
MPRK E Solution + 15893343.956 m
(mm)
40
20
0
-20
-40
?
2000
2001
2002
2003
2004
2005
2006

# Inter-Seismic Velocities

In chapter 2 I described an a priori tectonic setting for the East Sepik region based on a review of the literature. In chapter 3 I estimated velocities for ten sites spread across the region. Using the GPS velocities observed in this study combined with the velocities from three other sites at Vanimo (VANI) (*Tregoning et al.*, 2000), Bogia (BOGI) (*Wallace et al.*, 2004) and Jayapura (SENT) (*Bock et al.*, 2003), I am able to compare the a priori model with the observed model. The GPS sites are assumed from the a priori model to be situated on the following plates:

**North Bismarck:** KOIL and TARO

**South Bismarck:** BAMI and MUTM

**Block "A":** ANGR, TRNG, ABTI, MPRK, WEWK and XAVI

Table 4.1 shows that the observed GPS velocities do not match their estimated a priori rigid plate velocities. This may be a result of inter-seismic strain accumulation, errors in the rigid plate models or the existence of separate tectonic blocks. In this chapter I use elastic dislocation theory to present geophysical scenarios which explain the observed velocities.

## 4.1 Elastic Dislocation Theory

In elastic dislocation theory (ED), a fault is considered as a discontinuity across an otherwise continuous elastic medium (*Steketee*, 1958; *Healy et al.*, 2004). Such a discontinuity across a surface will result in two faces which can be deformed in different ways by the application of a force (*Steketee*, 1958). When the deformation force becomes greater than the applied force the elastic medium will spring back into a state of static equilibrium, which *Steketee* (1958) describes as a dislocation. ED theory provides a simple method by

which surface deformation from an earthquake can be estimated; resulting in the development of a number of different models (*Steketee*, 1958; *Chinnery*, 1961; *Savage and Hastie*, 1966; *Okada*, 1985).

One of the more common ED models is the model of *Okada* (1985) which describes the accumulation of elastic strain across a semi-infinite, homogeneous, isotropic medium. Displacements are provided in-terms of vectors, strain rates, and tilts with components ($U_1$, $U_2$, $U_3$) in a fault orientated coordinate system (Appendix B). The *Okada* (1985) model has the benefit, due to its simplicity, to be applied to a number of different situations where a reliable estimate of elastic strain accumulation or release is required (eg. *McCaffrey*, 2002; *Wallace et al.*, 2004; *Healy et al.*, 2004). A limitation of the *Okada* (1985) model is that a constant slip rate is assumed across the entire fault. It is widely recognised that displacement varies across the fault surface (*Kim and Sanderson*, 2005), hence a simple ED model will either over-estimate the displacement along the edges or underestimate the displacement at the centre. A way in which the displacement can be varied is to divide the main fault plane up into a number of sub-faults of smaller dimensions, across which the slip can be controlled. An example of this is shown by (*Delouis et al.*, 2004) for the Bourmerdes-Zemmouri earthquake, Algiers, where the main fault plane was subdivided into 40 smaller fault planes and co-seismic displacements inverted to obtain fault slip parameters. A disadvantage of using this method is that the number of fault parameters required increases with the number of fault planes, so care must be taken, particularly when inverting, to keep the model from becoming under-constrained.

ED theory is often used to model deformations associated with plate thrusting earthquakes, steady state plate subduction, and plate coupling. *Savage* (1983) proposed the use of ED theory to model the coupling effect across the plate boundary during the inter-seismic phase, by imposing a normal slip condition to the model, which he referred to as back-slip (Figure 4.1).

Back-slip modelling has been commonly used to account for inter-seismic strain accumulation at subduction zones (*Ruegg et al.*, 2002). Recent literature has criticised this use of ED theory. *Douglass and Buffett* (1995) argue that ED models, which are based on a kinematic formulation, place no constraints on subsurface stress fields leading to unreasonable distribution of stress at the subduction interface. *Zhao and Takemoto* (2000) strengthens the argument by comparing the use of three methods for estimating strain

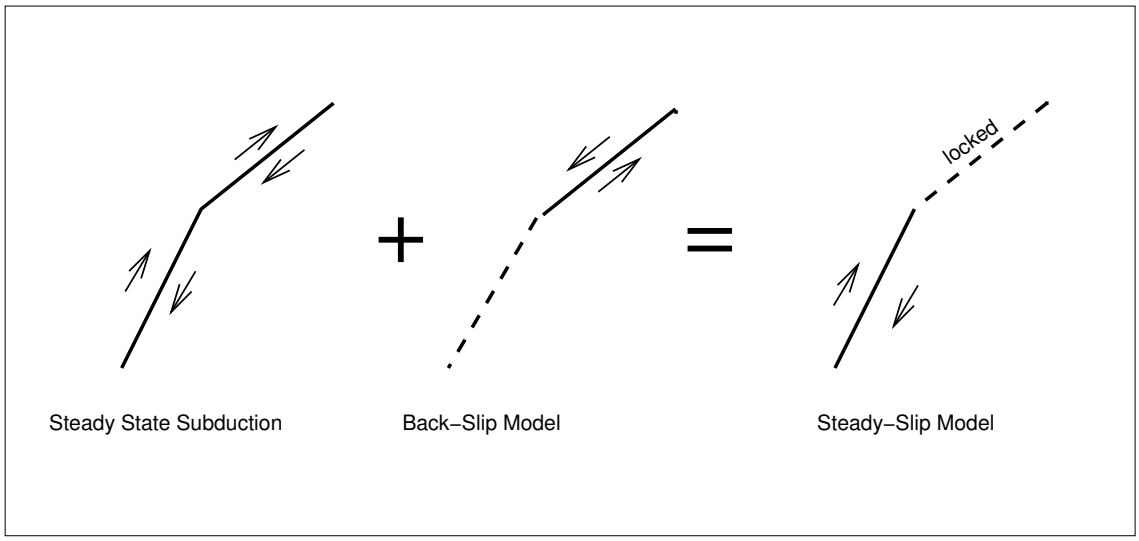


**Figure 4.1:** Dislocation model for plate coupling at a subduction zone (based on *Savage* (1983)). A steady-plate subduction model is added to a back-slip model (normal dip-slip equal to the plate convergence rate) results in a steady slip model for a locked plate interface (*Zhao and Takemoto*, 2000).

accumulation; reverse dip-slip, back-slip and a more complex synthesised model. As a result, *Zhao and Takemoto* (2000) state that a back-slip model cannot correctly predict horizontal motion of the subducted plate. *Williams and McCaffrey* (2001) show that the use of an ED model in a subduction environment is applicable in providing a good description of co-seismic displacements, but not suitable for investigation of inter-seismic stress changes, and suggest the use of a more complex strain accumulation model. *Savage* (1996) stated that, while ED models have many short comings when applied to a subduction environment, they are only intended to approximate deformation and have produced successful representations at many subduction zone environments (eg. *Savage et al.*, 1991; *Hyndman and Wang*, 1995).

In this study I use the ED model of *Okada* (1985) for a finite rectangular fault to investigate inter-seismic strain accumulation and estimate co-seismic displacements (Section 5.1.2). Despite the limitations that have been discussed, I use an ED model in a subduction zone environment (the NGT) due to the models simplicity and robustness to provide a reasonable first order approximation.

**Table 4.1:** Site Codes, Observed Absolute Site Velocities (ITRF2000) and Associated ($1\sigma$) Uncertainties. Sites are listed under their a priori plate and velocities with respect to my observations for this plate are also listed. Block "A" and additional sites are listed with respect to the Australian Plate.

| | Velocity (mm/yr) | | | | w.r.t Rigid Plate (mm/yr) | |
|---|---|---|---|---|---|---|
| Site | $v_e$ | $v_n$ | $\sigma_e$ | $\sigma_n$ | $v_e$ | $v_n$ |
| *North Bismarck Plate* | | | | | | |
| KOIL | -59.0 | 20.6 | 5.0 | 3.0 | 4.0 | 0.6 |
| TARO | -71.9 | 27.9 | 5.0 | 3.0 | 8.6 | 7.9 |
| *South Bismarck Plate* | | | | | | |
| BAMI | 19.9 | 32.5 | 5.0 | 2.8 | -30.1 | -16.5 |
| MUTM | 10.2 | 36.3 | 9.0 | 4.3 | -40.8 | -15.7 |
| *Block 'A'* | | | | | | |
| ABTI | 15.1 | 29.8 | 2.9 | 1.8 | -22.9 | -24.2 |
| ANGR | 25.1 | 46.7 | 3.4 | 1.7 | -12.9 | -7.3 |
| MPRK | 14.0 | 33.8 | 2.8 | 1.8 | -24.0 | -20.2 |
| TRNG | 24.4 | 47.7 | 3.0 | 1.8 | -13.6 | -6.3 |
| WEWK | 12.1 | 35.5 | 1.0 | 0.8 | -25.9 | -18.5 |
| XAVI | 0.0 | 60.0 | 7.0 | 1.0 | -38.0 | 6.0 |
| *Additional Sites* | | | | | | |
| VANI | 16.3 | 43.6 | 0.5 | 0.3 | -21.7 | -10.4 |
| BOGI | 26.5 | 42.8 | 1.9 | 1.6 | -11.5 | -11.2 |
| SENT | 10.2 | 37.7 | 1.5 | 0.6 | -27.8 | -16.3 |

## 4.2 Inter-Seismic Scenarios

The GPS sites observed in this study show motion that is not consistent with their observed a priori plates. The variations at these sites indicate that either, the a priori model is incorrect or that they are being influenced by other tectonic signals (eg. inter-seismic strain or post-seismic relaxation). Here I describe possible geophysical scenarios which explain the observed misfits.

### 4.2.1 The North Bismarck Plate

The sites KOIL and TARO are situated on the NBP near the junction of the NGT and BSSL. The observed GPS velocities for these sites match the rigid NBP velocity estimated by *Tregoning* (2002) at 95% confidence (Table 4.1). Velocity estimates were made for these sites using only observations from the 2003 and 2004 campaigns, as the time series show non-linear trends after PNG02 (Section 3.3). I discuss here two possible explanations:

- The sites display a co-seismic discontinuity due to an event between late 2002 and late 2003.
- The sites are undergoing post-seismic relaxation after PNG02.

The hypothesis that the sites were displaced as the result of an event between late 2002 and late 2003, would break the non-linear trends into two linear trends separated by a discontinuity. If this were the case the displacements would be (-24 $\pm$15mm E, -26 $\pm$8mm N) at TARO and (-13 $\pm$14mm E, -18 $\pm$6mm N) at KOIL. Using the formalisation of *Okada* (1985) an ED displacement field can explain the displacements to be a thrust event of $M_w \approx 6$, located at 3.34°S, 144.21°E (Appendix C). A search of the Harvard CMT catalogue revealed two events to have occurred within this time period, but they do not fit the required parameters, hence this scenario is not likely.

The second hypothesis that the sites are undergoing post-seismic relaxation appears more plausible as both XAVI and WEWK have been shown to fit an exponential decay curve, which is indicative of post-seismic relaxation (*Savage and Svarc*, 1997) (Section 3.3). Post-seismic deformation has also been shown to fit a logarithmic function (*Hearn*, 2003). However, the observed motion at TARO and KOIL do not fit either type of decay curve. This does not discount that the sites are undergoing post-seismic deformation; further GPS observations may be able to provide a better indication of the situation. The inter-seismic velocities which will be assumed for TARO and KOIL have been made from a linear fit between the observations made during 2003 and 2004, as they best represent the estimated rigid plate motion of th NBP (Table 3.2).

### 4.2.2 Coupling across the Bismarck Sea Seismic Lineation

The sites MUTM and BAMI are located near the BSSL on the northern edge of the SBP. Velocity estimates at these sites were made after PNG02 and differ from the rigid SBP velocity estimated by (*Tregoning et al.*, 1999) (Table 4.1). To explain the observed variances I show that significant coupling is present across the BSSL.

*Wallace et al.* (2004) state a need to account for inter-seismic strain accumulation at GPS sites in PNG, due to the close proximity of active fault boundaries. Figure 4.2 shows the results of back-slip modelling across the BSSL assuming a 100% rate of coupling at the fault interface. The predicted rates of strain accumulation explain the observed GPS velocities to within 95% confidence (Figure 4.2). The relative motion applied in the back-slip

model (130 mm/yr along-strike and 30 mm/yr convergence) was based upon estimates by *Tregoning* (2002).

Justification for there being a significant rate of coupling across the BSSL can be shown by looking at the seismic activity across the western extent of the fault. The BSSL is a seismically active fault with at least one strike-slip event occurring along the western extent every year. As earthquakes occur when the elastic force surrounding a fault becomes greater than the static coupling force (*Cox and Hart*, 1986), the BSSL region would be likely to have a significant rate of coupling. Further observations at these sites would help provide a better estimate of the inter-seismic accumulation of elastic strain.

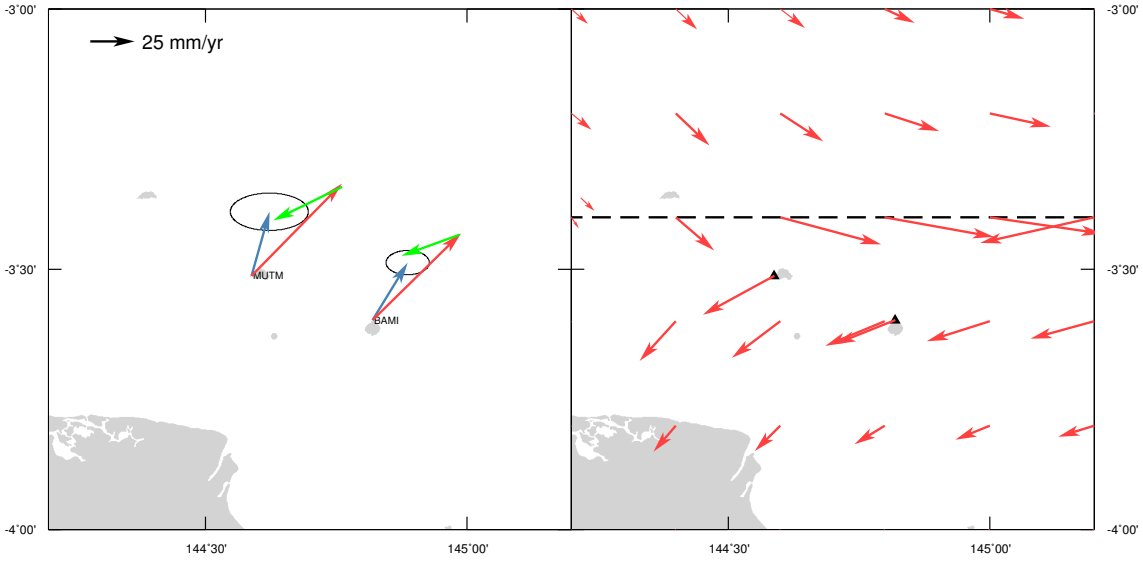


**Figure 4.2:** (Left) The fit between the observed (blue), rigid plate (red) and inter-seismic strain (green) velocities. (Right) The deformation field for elastic strain accumulation across the BSSL.

### 4.2.3 A Separate Tectonic Block?

*Tregoning et al.* (2000) showed that GPS observations from the sites WEWK, VANI and ANGS had observed velocity estimates that were a consistent 30% slower with a 10°rotation than the estimated rigid Australian Plate velocity. They indicated this to be either a result of inter-seismic strain accumulation or a separate tectonic block. The observations from this study made at WEWK, ABTI, TRNG, MPRK and ANGR show similar variations from the rigid Australian Plate (Figure 4.3). In my a priori model I accommodated for non-rigid plate movement in this region by introducing a Block "A", which was described as displaying tectonic signals that are a combination of the rigid Australian

Plate and the New Guinea Highlands Plate. In this section I propose three hypothesis to test the the fit of Block "A" to estimated rigid plate movements:

- Block "A" displays rigid Australian Plate motion.
- Block "A" displays rigid New Guinea Highlands Plate motion.
- Block "A" displays its own rigid plate motion.

Figure 4.3 shows the observed motion of the Block "A" sites with respect to the rigid Australian Plate as estimated by *Tregoning* (2002). The variation from rigid plate motion could be a result of inter-seismic strain accumulation across the NGT, which was known to be experiencing seismic coupling due to the PNG02 earthquake occurring. To test this, I applied a back-slip model using the formalisation of *Okada* (1985). Models were created using varying gradients of coupling along-strike and down-dip between 0 and 100% (Figure 4.4), however no combination resulted in a fit between the locked, rigid plate and the observed GPS velocities. This is a clear indication that Block "A" is not displaying rigid Australian Plate motion.

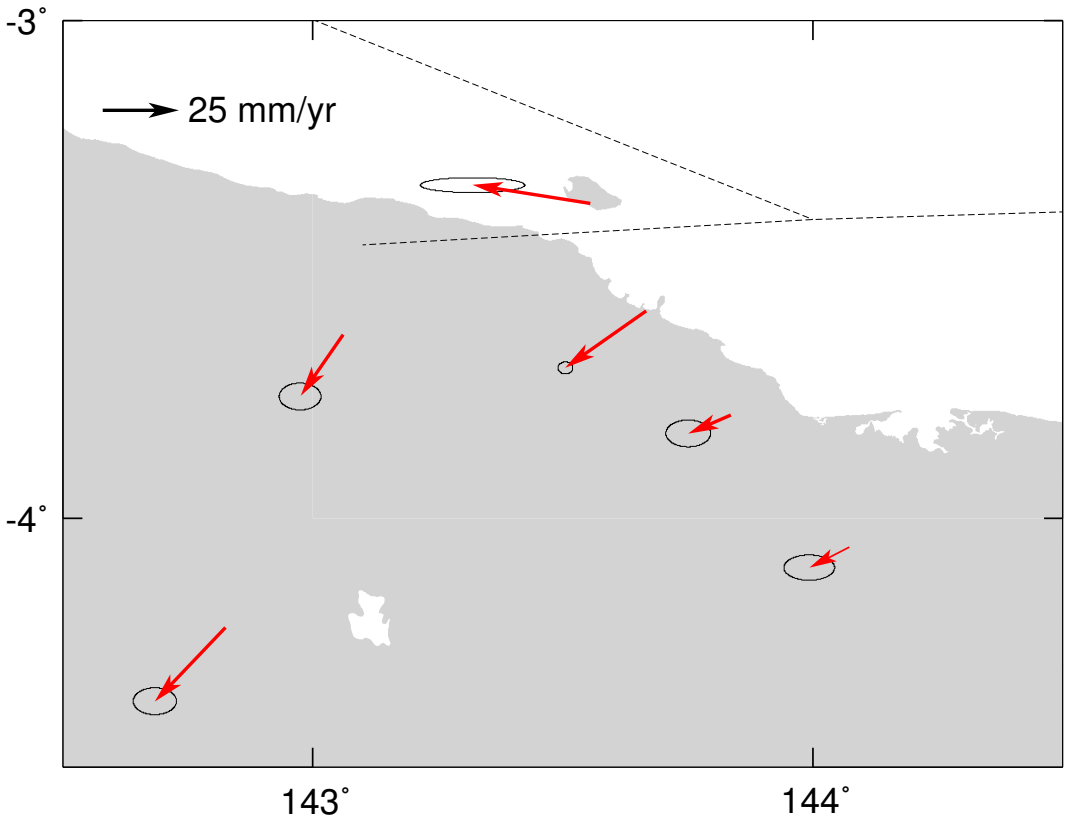


**Figure 4.3**: Observed site velocities relative to the rigid Australian Plate.

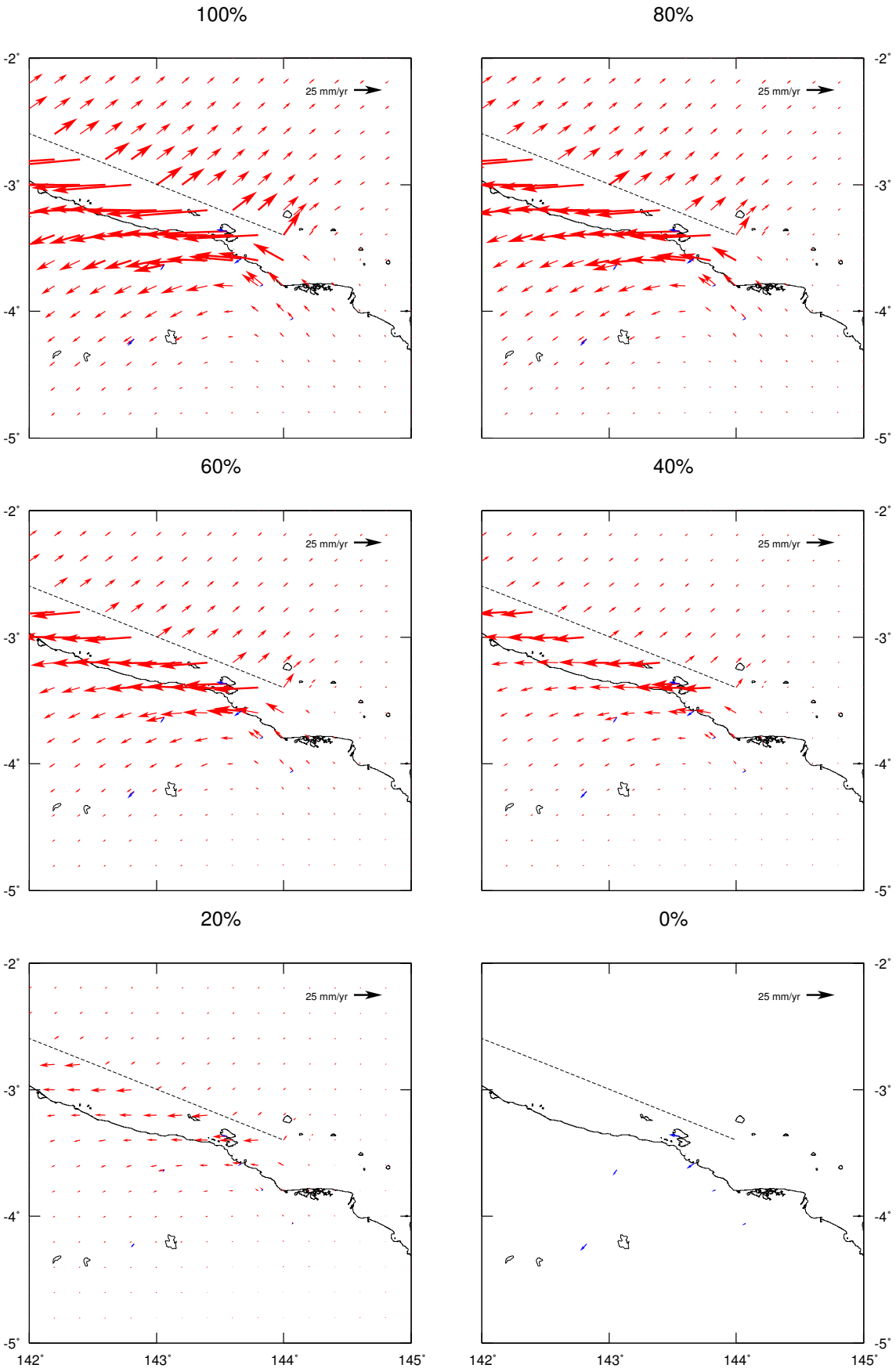


**Figure 4.4:** Back-slip models for coupling across the New Guinea Trench at varying gradients between 0 and 100% (red). Also shown are the estimated velocities of the GPS sites relative to the rigid Australian Plate (blue). The back-slip vectors here do not explain the variances between the observed site velocities and rigid Australian Plate velocity.

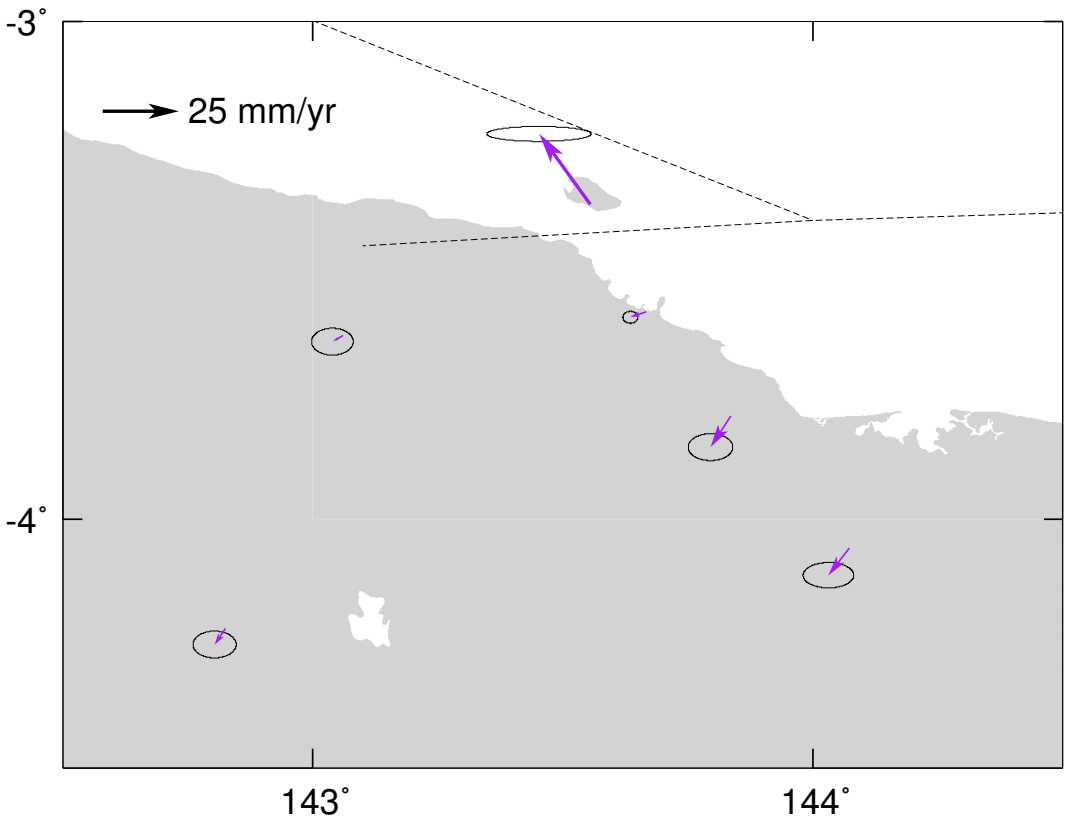


**Figure 4.5**: Observed site velocities relative to the rigid New Guinea Highlands Plate.

*Wallace et al.* (2004) proposed the existence of a rigid New Guinea Highlands Plate. The northwestern extent of this plate is at present undefined but *Wallace et al.* (2004) suggest the possible extension north to the NGT and west into Irian Jaya. Figure 4.5 shows the observed motion of the Block "A" sites with respect to the NGH Plate. I calculated the Euler pole of the NGH Plate relative to the ITRF2000, from the AUS/NGH and ITRF00/AUS Euler poles provided by *Wallace et al.* (2004) (Table 2.2). The observed GPS velocities at the sites ABTI, MPRK, WEWK match the estimated rigid NGH Plate velocity within 95% confidence. However, I am somewhat sceptical of these results as they do not account for the influence of elastic strain accumulation across the fault, and under-estimate the velocities at ANGR and TRNG.

The sites ANGR and TRNG are both far enough from the NGT for the influence of inter-seismic strain to be minimal (Figure 4.4). The observed velocity estimates for TRNG and ANGR are similar to estimates made at BOGI (*Wallace et al.*, 2004), which is ∼100km east of ANGR. This provides justification to assume that ANGR, TRNG and BOGI are displaying the rigid velocity for the Sepik region (Block "A"). Figure 4.7 shows the observed motion of the Block "A" sites with respect to the velocity estimate at ANGR. However, a

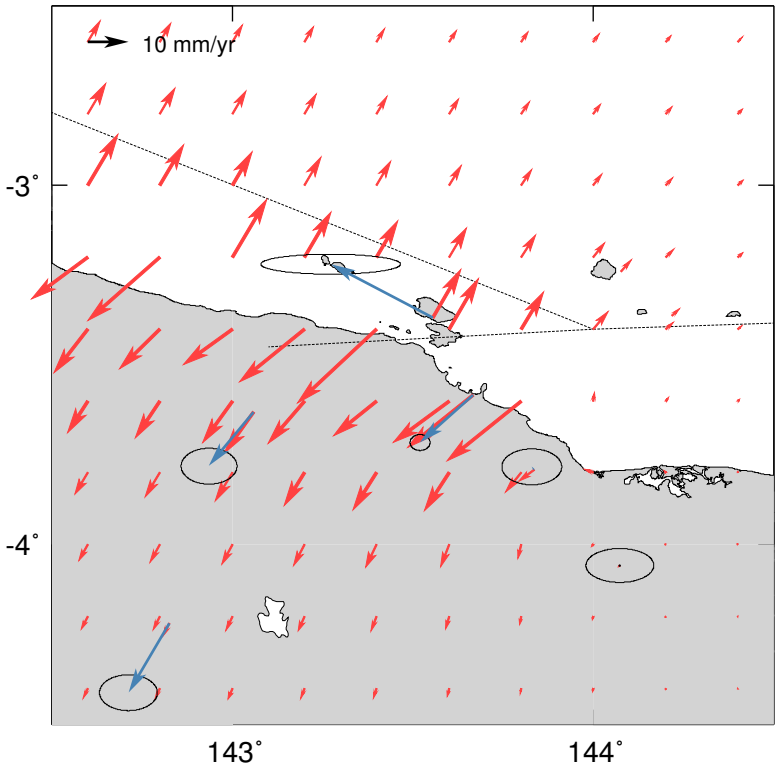


**Figure 4.6:** Back-slip models for coupling across the New Guinea Trench at showing coupling of 20% along-strike and 90% down-dip, for Block "A". Also shown are estimates of the velocities of the GPS sites relative to the velocity at ANGR (blue).

variance in velocity is shown at WEWK, MPRK and ABTI. Using the new velocity estimate for the relative motion across the NGT, between the rigid NBP and ANGR, a back-slip model (20% coupling along-strike and 90% coupling down-dip, Figure 4.6) is shown to accommodate this variance. Figure 4.8 shows the observed motion of the Block "A" sites, corrected for interseismic strain accumulation with respect to the velocity estimate at ANGR. This model explains the observed motion at all of the sites except ABTI, which is situated 130 km from the NGT and has only been occupied twice. However the velocity estimates at ABTI are consistent with MPRK which was observed during the same campaigns. Further geodetic data from these sites is required to explain this.

### 4.2.4 A Velocity Estimate at Kairiru

The GPS site XAVI is situated on the island of Kairiru, about 19km north of Wewak (Figure 3.1). The site is observed to display non-linear motion in the east component, which fits an exponential decay curve, indicating possible post-seismic relaxation. No velocity estimate could be made at XAVI before PNG02, hence the east component is shown to have an inter-seismic velocity of $0 \pm 7$ mm/yr, which is derived from the asymptotic be-

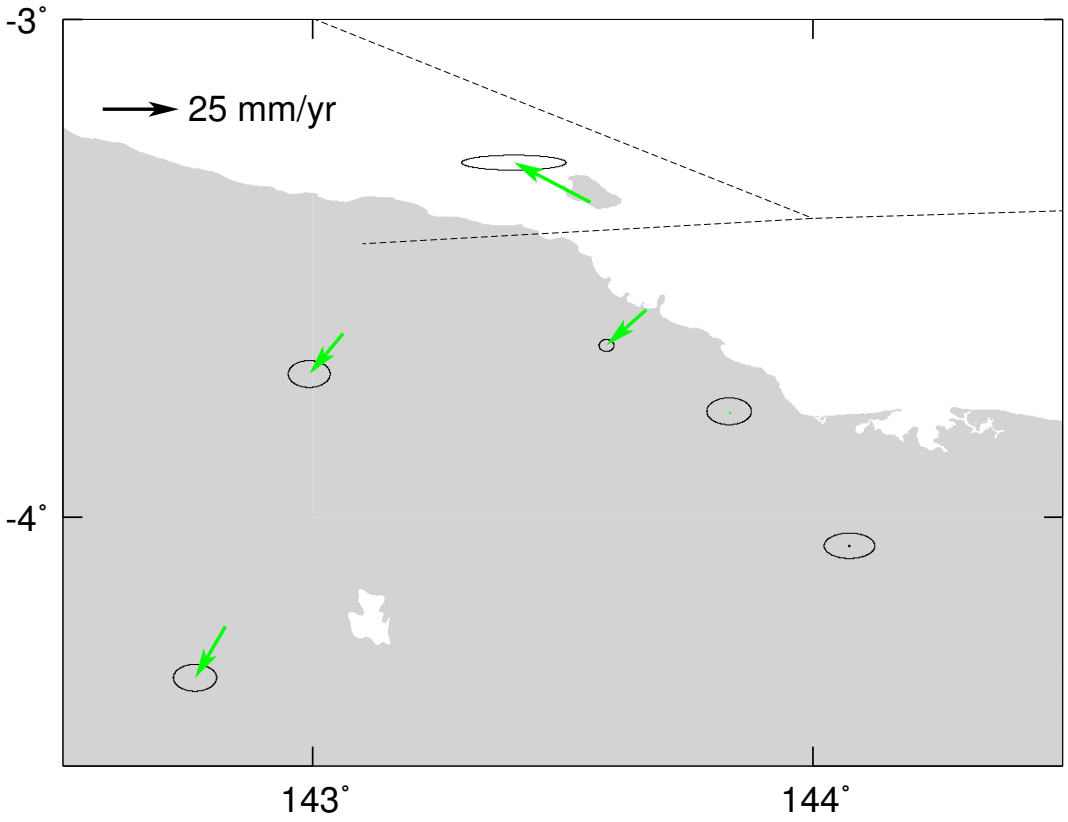


**Figure 4.7**: Observed site velocities relative to Block "A" (ANGR).

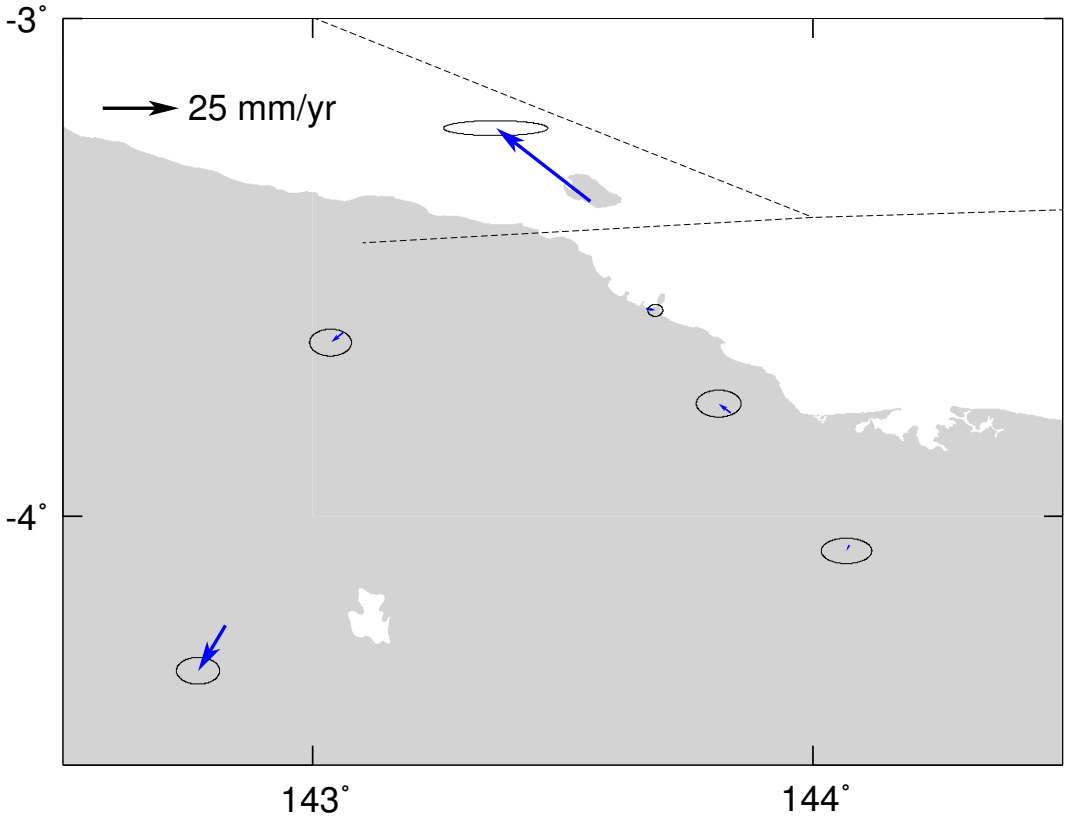


**Figure 4.8:** Observed site velocities relative to Block "A" (ANGR) which have been corrected for inter-seismic strain accumulation.

haviour of the exponential curve. In the north component the observed motion is linear, however the velocity estimate is significantly greater in magnitude than the surrounding sites (XAVI, MPRK and TRNG). Figures 4.3,4.5 and 4.8 show that XAVI does not display rigid plate motion that is consistent with the Australian, New Guinea Highlands or Block "A". So on what plate is XAVI situated?

The GPS observation at XAVI are currently insufficient to conclude why the site does not display motion that is consistent with the a priori tectonic setting of the region. A possible explanation is that some authors (eg. *Cooper and Taylor*, 1987; *Klootwijk et al.*, 2003) have postulated on the extension of the BSSL westward across PNG (Section 2.1.1) which would run between XAVI and WEWK. This would indicate that XAVI may be situated on a separate tectonic block wedged between the NGT and BSSL (Block "B"?). To justify the existence of such a tectonic block more geodetic observations are required.

## 4.3 Summary

The analysis of possible geophysical scenarios has yielded the following explanations:

- TARO and KOIL display non-linear motion that is most likely caused by post-seismic relaxation.
- The BSSL was locked between 2003 and 2004 with large rates of inter-seismic strain being observed at MUTM and BAMI.
- The East Sepik region appears to be moving as a separate tectonic block (Block "A"), but current GPS observation are inconclusive as to the definition of this motion.
- Inconclusive observations at XAVI support evidence that the BSSL continues west across New Guinea, suggesting the existence of a separate tectonic block wedged between the NGT and BSSL (Block "B"?).

# Earthquake Deformation

It is widely recognised that large earthquakes cause the redistribution of strain and stress across a region (*Cox and Hart*, 1986). Such deformation occurs in three distinct phases; inter-, co-, and post-seismic (*Scholz*, 2002). To estimate the surface displacements at the time of an earthquake (co-seismic), the displacement of the Earth's surface before (inter-seismic) and after (post-seismic) the event must be known (*Reilinger et al.*, 2000).

This chapter is divided into two sections; in the first I describe the effect of the observed post-seismic relaxation across the region and estimate co-seismic displacements. In the second part I invert the estimated co-seismic displacements to estimate fault geometry and slip parameters for PNG02.

## 5.1 Surface Deformation

During the earthquake, which was interpreted by the Harvard CMT solution to be a low angle thrust event, the NBP Plate was over-ridden by Block "A", with a slip estimated by *Borrero et al.* (2003) of 2.1m. The pattern of inter-, co- and post-seismic deformation for a typical thrust event is illustrated in Figure 5.1.

### 5.1.1 Post-Seismic Relaxation

Post-seismic relaxation is shown to be occurring at the sites XAVI and WEWK (Section 3.3). This phase is due to either a visco-elastic response to the deformation within the Earth or afterslip across the fault, and is best represented by a decay curve (*Cox and Hart*, 1986). In this study I have fitted the deformation occurring at XAVI and WEWK with an exponential curve as described by (*Savage and Svarc*, 1997). The post-seismic relaxation generally occurs in the same direction as the co-seismic displacements. At WEWK and XAVI, the co-seismic displacements occurred in an easterly direction, consistent with the

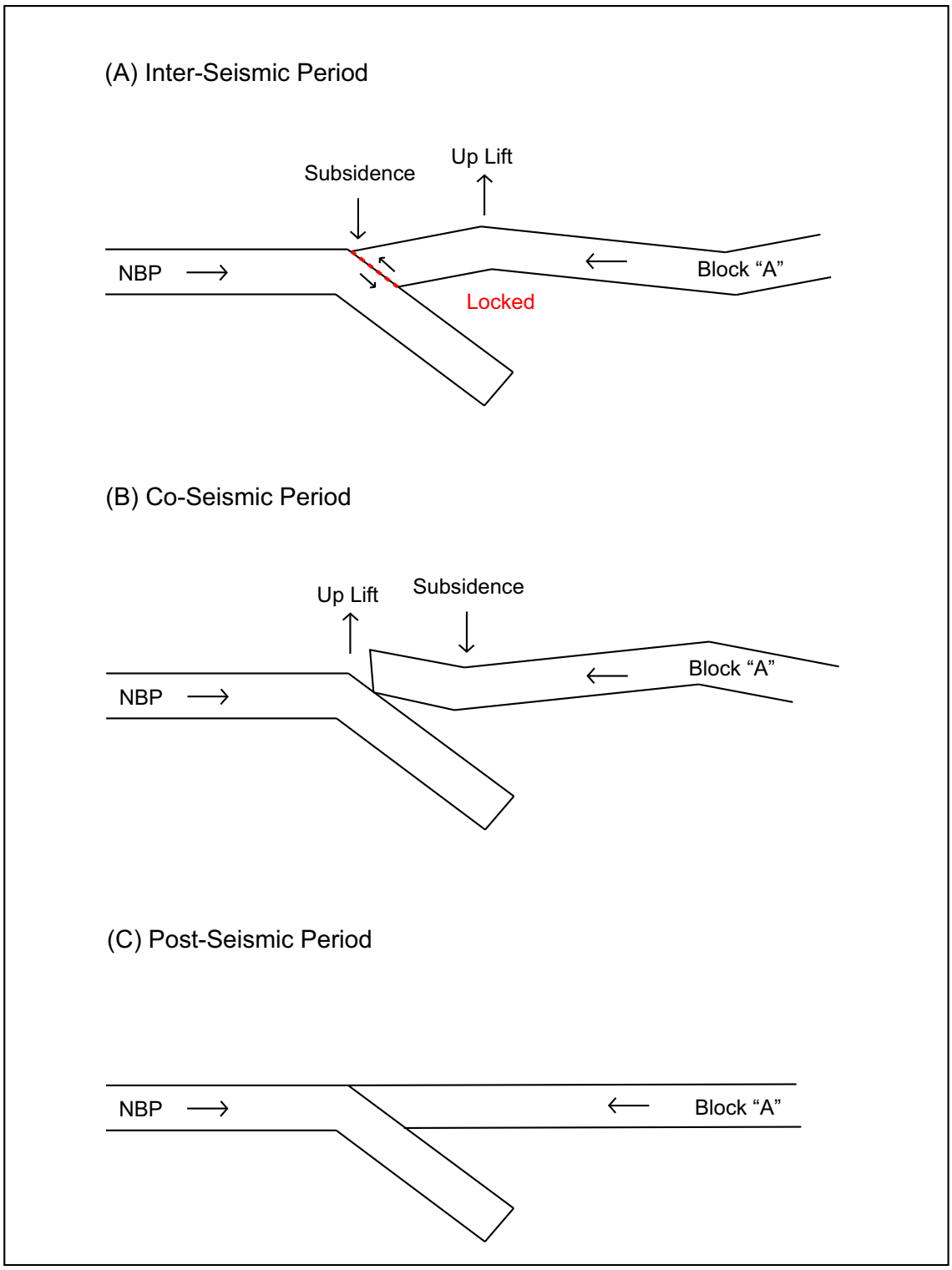


**Figure 5.1:** Illustration of a thrust earthquake at a subduction zone. (a) During the inter-seismic phase locking occurs across the subduction interface, this producing elastic strain accumulation across the fault. (b) Deformation during the co-seismic phase results in uplift of the hanging wall (over-riding plate) at the trench. (c) After the co-seismic rupture, a post-seismic phase is observed while the fault returns to a static state.

observed post-seismic relaxation. The exponential curve fitted to XAVI displays linear motion during mid 2006, indicating a post-seismic period of about 4 years. Over this period the magnitude of deformation is estimated to be ∼120 mm at WEWK and ∼80 mm at XAVI. The estimate of deformation at WEWK is potentially inaccurate due to the time parameter from XAVI being used to fit the curve.

In section 4.2.1 I indicated the likelihood of post-seismic motion at TARO and KOIL, the justification of this proved inconclusive due to the data fitting neither an exponential nor a logarithmic curve. Not being able to explain the post-seismic movement at these sites does not result in a significant change to the co-seismic estimates, as the two sites were occupied immediately after PNG02. The remainder of the GPS sites have insufficient observations to resolve whether post-seismic signals are present or not.

### 5.1.2 Co-Seismic Displacement

Co-seismic displacement is the movement of a site at the time of an earthquake (Figure 3.3) (*Scholz*, 2002). The co-seismic displacements estimated from the GPS observations in this study are shown in Figure 5.2 (also Table 5.1). I calculated the displacements by first extrapolating the estimated inter-seismic velocities from before and after[1] the event to the time of the event and differencing the resulting positions. The post earthquake positions at XAVI and WEWK were corrected for the observed post-seismic movement (Section 5.1.1).

In this study, only eight GPS sites have observed co-seismic displacements. In order to keep the model well constrained it is essential that these estimates be reliable. This raises the question of how does one assess the accuracy of an estimate of co-seismic displacement? Co-seismic displacement is generally seen as the instantaneous change in position (*Chlieh et al.*, 2004), hence the most reliable estimate would be to have observations immediately before and immediately after the earthquake. This is not always possible, as the majority of GPS studies (including this one) are not observed continuously, but at intervals, spanning a number of years. In this study, observations were made at the closest sites to the rupture (WEWK, TARO, KOIL, XAVI and TRNG) within a week of PNG02. Of these sites TRNG and WEWK were observed four months before PNG02; hence, these

[1] Due to insufficient observations, it is not possible to estimate velocity both before and after the earthquake; therefore, for all sites, the velocity before the earthquake is assumed to be the same as the velocity estimated after earthquake, shifted to fit the observed GPS data.

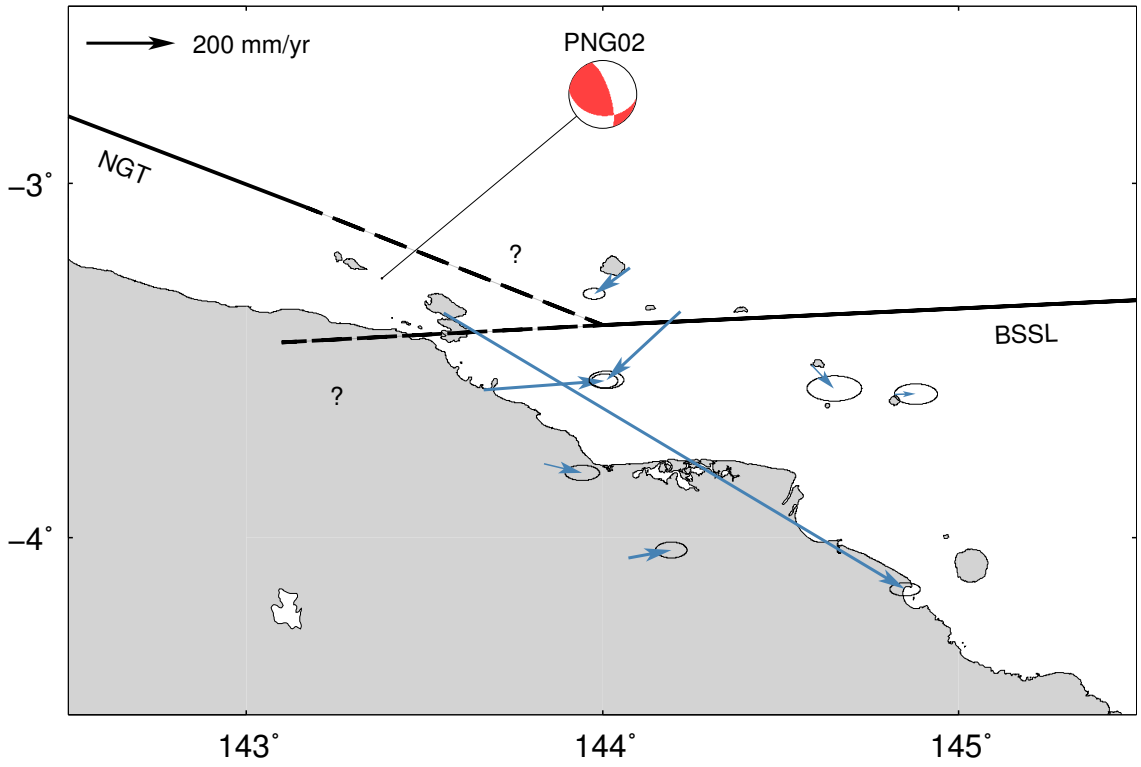


**Figure 5.2:** Observed co-seismic displacements from this study (blue). Also shown is the Harvard CMT focal mechanism for PNG02 (red).

sites have the most reliable estimates of co-seismic displacement. This measure of reliability is not shown by the formal uncertainties, which have been provided in this study to show the accuracy of the displacements (Table 5.1). These uncertainties are based on those provided by GLOBK for the position estimates and have been propagated through the data reduction. Hence they are generally observed to be four times larger than those of the position estimates.

## 5.2 Non-Linear Inversion with the Neighbourhood Algorithm

Many scientific problems use models with well constrained parameters to make predictions about a specific observable. Inverse modelling is an iterative process that uses a set of observables to infer the actual model parameters (*Tarantola*, 2005). The inversion of displacement fields using ED theory to obtain fault geometry and slip parameters is not a new concept and has been used successfully in a number of subduction zone environments (eg *McCaffrey*, 2002; *Delouis et al.*, 2004).

To invert the co-seismic displacements estimated in this study into a suitable set of fault

**Table 5.1**: Co-seismic displacements from this study with $2\sigma$ formal uncertainties.

| | Disp. (mm) | | Uncert. (mm) | |
|---|---|---|---|---|
| Sites | East | North | East | North |
| ANGR | 95 | 17 | 28 | 14 |
| BAMI | 48 | 1 | 38 | 18 |
| KOIL | -166 | -154 | 32 | 16 |
| MUTM | 50 | -53 | 50 | 22 |
| TARO | -80 | -59 | 20 | 10 |
| TRNG | 85 | -21 | 30 | 14 |
| WEWK | 271 | 20 | 24 | 12 |
| XAVI | 1035 | -620 | 28 | 14 |

parameters, I have applied the Neighbourhood Algorithm (NA), which was introduced by *Sambridge* (1999a,b) as a direct search method for non-linear inversion. The NA was specifically designed for geophysical problems and works in a two stage process. In the first stage, a search algorithm uses Voroni cells (nearest neighbour regions) to define a uniform random walk through a multi-dimensional parameter space to select a suitable set of model parameters (*Sambridge*, 2002). The second stage is an appraisal stage where a rank is used to extract the "best" model based on a specified set of conditions (*Sambridge*, 1999a).

I have combined the NA with a forward ED model based upon the *Okada* (1985) algorithm for ED across a finite rectangular fault. The *Okada* (1985) model is used to estimate a displacement field from a given set of fault parameters, while the NA aims to recover fault parameters from indirect measurements, which in this case are the observed co-seismic displacements. As a result of the inversion process, a best-fitting set of fault parameters and corresponding displacement field is obtained. Figure 5.3 shows a flowchart of the inversion procedure.

The model is set up to search for eight parameters (length, latitude, longitude, slip along-strike, slip down-dip, strike, dip and locking depth) constrained by user-specified ranges. The model has the option for further constraint by holding the moment magnitude fixed at a user-specified value. When this option is turned on, the width of the fault (length down-dip) is calculated within the program based on the slip and length (Equation 5.2, where $\mu$, the shear modulus = $3 \times 10^{11}$ dyne-cm$^{-2}$ ). The NA recovers the best fitting model by using a rank or misfit given to each forward model. I define the misfit as the weighted sum of the squares of the difference between the observed and the computed displacement fields (Equation 5.3).

$$M_w = (\frac{2}{3}\log_{10} Moment) - 10.7 \tag{5.1}$$

$$Moment = \mu \times Length \times Width \times Slip \tag{5.2}$$

$$misfit = \sum_{i=1}^{N} \left( \frac{observed_i - computed_i}{weight_i} \right)^2 \tag{5.3}$$

Inverse models are both sensitive and tractable (*Healy et al.*, 2004). The co-seismic displacements estimated in this study range in magnitude from 1 mm to 1000 mm and, the significantly large magnitudes tend to dominate the inversion. As a best fitting model must aim to explain displacements at all sites, I have weighted the observations based on the formal $2\sigma$ uncertainty divided by the observed displacement. The weight is used in Equation 5.3 to calculate the misfit and rank the model.

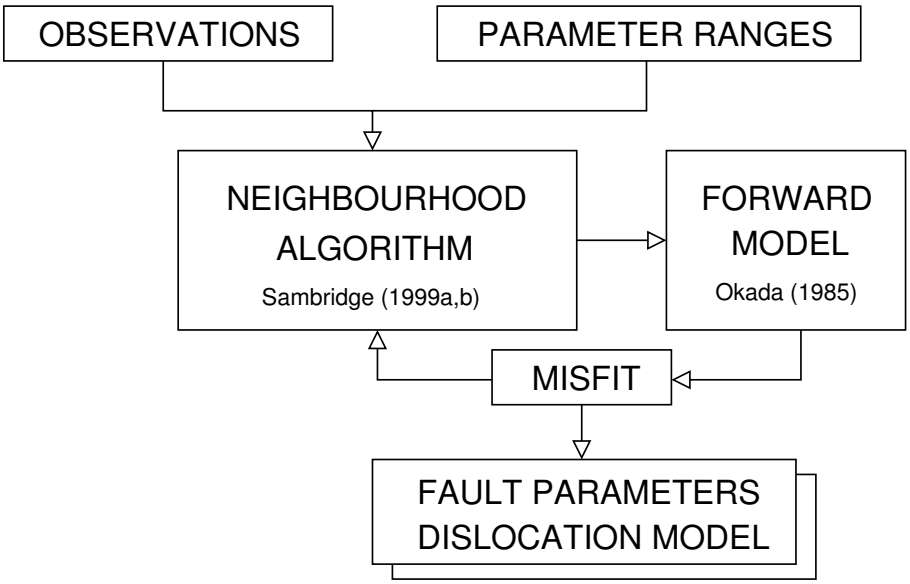


**Figure 5.3:** Flowchart of the non-linear inversion based upon the Neighbourhood Algorithm (*Sambridge*, 1999a,b) and the *Okada* (1985) Elastic Dislocation model. Input to the model are ranges for eight parameters and moment magnitude. Output of the model is a displacement field and fault geometry and slip parameters.

## 5.3 Results

Previous interpretation of the rupture process for the PNG02 has been made by *Borrero et al.* (2003), who describe a length, width and slip of the fault based upon the Harvard CMT solution. In this interpretation *Borrero et al.* (2003) use *Okada* (1985) model to compare the fault parameters with observed up-lift and subsidence measurements reported by *Davies* (2002) and *Davies et al.* (2002). The predicted uplift rates are shown to be consistent. In this study I have reproduced the ED model described by *Borrero et al.* (2003), using the same *Okada* (1985) model and same fault geometry and slip parameters (Table 5.2)(here after this model will be referred to as "Model 0").

Figure 5.4a shows a comparison between the computed surface displacements of "Model 0" and the estimated co-seismic displacements of this study. It is clear that the two estimates are not consistent. To reconcile the conflicting data sets I ask three questions:

- Can the observed GPS displacements be described by a single rupture?
- Does this model explain the observations of uplift and subsidence reported by *Davies* (2002) and *Davies et al.* (2002)?
- Is this model geophysically plausible?

### 5.3.1 GPS Displacement Model - "Model 1"

Using the NA and ED model of *Okada* (1985), I inverted the estimated horizontal co-seismic displacements, using a set of loosely constrained fault parameters. The option to constrain the moment magnitude was turned off. The solution was iterated 250 times, with each iteration containing 150 models. The resulting model explained the co-seismic displacements at five sites (XAVI, WEWK, TARO, KOIL, and TRNG) (Figure 5.4b). It is interesting that sites which did not fit the estimated displacement field (ANGR, BAMI and MUTM), were the sites at which observations were not made immediately after PNG02.

### 5.3.2 Comparisons and Constraints

"Model 1" describes a shallow, steep dipping thrust event to have initiated at -3.30°S, 143.42°E and propagated for 92 km along the NGT. This event is consistent with the estimated co-seismic displacements, but displays a different rupture pattern to the previously published "Model 0". The main differences between the two models are the

location of the event, the dip angle, the magnitude of the slip and moment. These differences do not mean that "Model 1" is in error, but must be justified in order to describe the model as being geophysically plausible.

The estimated location of "Model 1", shows that the rupture propagated south-east and extended for about 50 km passed the a priori location for the junction between the NGT and the BSSL. The fact that the trench ruptured across an assumed fault boundary indicates that there might be some inaccuracy in this estimate. Two explanations for this are that the subducting slab is deeper here than the depth of the BSSL, hence the rupture occurred underneath the BSSL; this is unlikely due to the estimated parameters indicating the trench ruptured to the surface. The second explanation is simply that the BSSL does not extend westward as postulated by *Cooper and Taylor* (1987) but stops at $\sim$144°E as suggested by *Hamilton* (1979) and *Johnson* (1987). This explanation would contradict the evidence already presented in this thesis that the GPS site XAVI is wedged between the BSSL and NGT. The justification of the estimated location of the fault, does not look likely, but sufficient evidence does not exist to suggest otherwise.

The slip estimated by the inversion is 60% greater than that used in "Model 0", which *Borrero et al.* (2003) obtained using the scaling laws of *Geller* (1975). In this model the slip is used as justification of the moment magnitude, which was under-estimated in "Model 1". The moment magnitude is related to the slip, the area of the fault and the rigidity (shear modulus) of the surface (Equation 5.2). Initially I used a value for rigidity of $3 \times 10^{11}$ dyne-cm$^{-2}$ which is an accepted value for rock (*Scholz*, 2002). When I apply this calculation to the parameters described in "Model 0" the resulting moment is 60% smaller. This indicates that to calculate the slip across the fault *Borrero et al.* (2003) appears to have used a rigidity value of $\sim 5 \times 10^{11}$ dyne-cm$^{-2}$, which is consistent with rigidity values that have been used for large earthquakes in the Indonesian region (eg. *Liu*, 2005). Using this rigidity value I recalculated the moment magnitude of the estimated parameters from "model 1" to be $M_w$ = 7.6, which is consistent with the Harvard CMT estimate.

"Model 1" is estimated to be a steep dipping (62°) event. The dip in this region of the NGT is indicated from tomographic imagery by *Tregoning and Gorbatov* (2004) to be $\sim$10°, which is consistent with "Model 0." Looking at the the tectonic setting of this region, I would speculate that there would be considerable variation in dip along the fault plane described by "Model 1." *Johnson* (1987) suggest that the NGT merges with the BSSL in

a fault - trench junction. The BSSL is shown to have a near vertical dip, hence before merging, the NGT would need to increase in dip. There are insufficient observations across the region to justify this and the *Okada* (1985) ED model is limited in the sense that it cannot account for a varying dip angle across the rupture. A way of modelling a varying dip angle would be to split the fault into sub-faults, which for this study could result in an under-constrained inversion model (Section 4.1).

After the earthquake and tsunami a survey was conducted to make measurements of uplift and subsidence, but no horizontal displacements were recorded (*Davies*, 2002). "Model 0" was based entirely on the results of this survey (*Borrero et al.*, 2003), which show consistent uplift of 30 - 40 cm across the near shore islands and subsidence of 10 - 20 cm was observed long the coast near Hawain. Figure 5.4a and 5.4b show the predicted vertical displacements of "Model 0" (which is consistent with the observations) and "Model 1". It is clear that "Model 1" is not consistent with uplift across the islands of Tarawai and Walis nor the subsidence observed near Hawain. However, subsidence is shown offshore between Kairiru. The pattern of vertical deformation shown by "Model 1" differs considerably from "Model 0", but is consistent with the estimated pattern for vertical deformation at an oblique subduction zone (*Bevis and Martel*, 2001). Therefore, in order to completely describe the rupture the measured uplift and subsidence measurement must be accounted for.

**Table 5.2:** Estimated Fault Geometry and Slip Parameters from the interpretation of *Borrero et al.* (2003) and the for the inversion of this study. * The moment magnitude from "Model 1" was recalculated to be 7.6 using the same rigidity values as *Borrero et al.* (2003).

| | Model 0 | Model 1 | Model 2 |
|---|---|---|---|
| Latitude | -3.27° | -3.3° | -3.15° |
| Longitude | 142.95° | 143.42° | 142.95° |
| Length (km) | 72 | 92 | 72 |
| Width (km) | 36 | 10 | 29 |
| Strike | 106° | 114° | 112° |
| Dip | 34° | 62° | 30° |
| Rake | 43° | 39° | 55° |
| Co-Seismic Slip (mm) | 2100 | 3384 | 2624 |
| *along-strike* | 1432 | 2613 | 2160 |
| *down-dip* | 1535 | 2151 | 1500 |
| Moment Magnitude ($M_w$) | 7.6 | 7.3* | 7.6 |

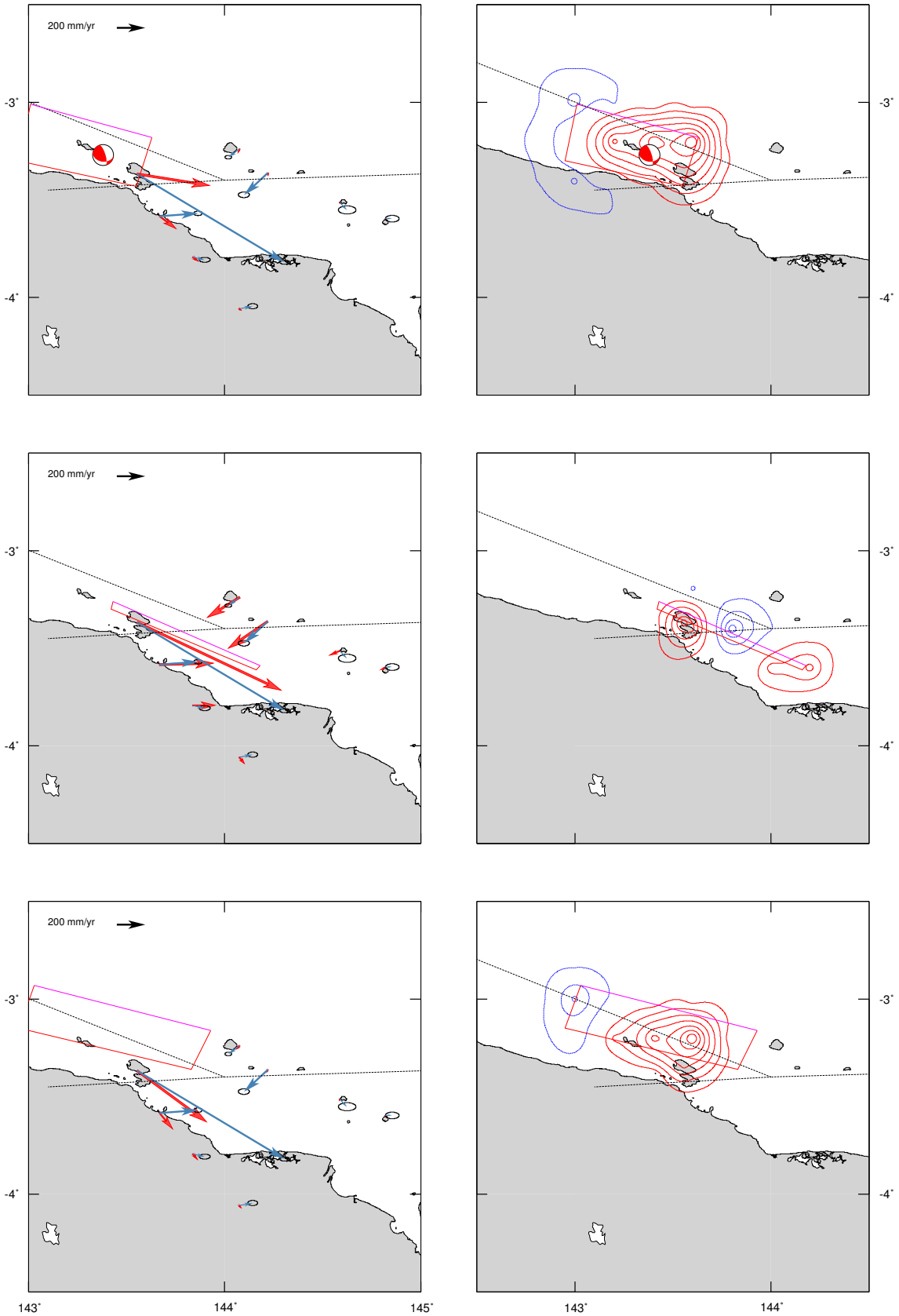


**Figure 5.4:** (Left) Predicted co-seismic displacements from (top) "Model 0" (middle) "Model 1" and (bottom) "Model 2" compared with the estimated co-seismic displacements from this study. Also shown are the estimated fault planes for the three models (Right) the predicted uplift and subsidence for the three models. The contours were estimated by a 0.2°grid and are placed at 0.1 m intervals. The red contours indicate uplift and the blue contours indicate subsidence.

### 5.3.3 Vertical Displacement Model - "Model 2"

In a second attempt to reconcile the conflicting data sets, I added vertical constraints to the inversion based on measurements of uplift and subsidence reported by *Davies* (2002). Furthermore, I have added some of the estimated vertical displacements from the GPS data set. Some of the GPS time series show erratic variations in the heights, most likely caused by errors in antenna height measurements used in the reduction of the GPS observations (not all field notes were available to verify these values). The time series at WEWK, XAVI and TRNG are reasonably consistent and clear co-seismic displacements can be identified. The model was also constrained by fixing the moment magnitude at $M_w = 7.6$, which is the Harvard CMT estimate for the event. The solution was iterated 250 times, with each iteration containing 150 models. The result showed uplift that was consistent with "Model 0"; a maximum uplift of 0.7m was predicted just offshore of Kairiru (Figure 5.4c). The predictions of subsidence at Hawain were not as great as those predicted by "Model 0" or as observed by *Davies* (2002).

The predictions of horizontal surface displacements made by "Model 2", do not provide a significantly better match than "Model 0." One difference is that direction of displacement at XAVI is better predicted, but the magnitude is only half of the observed GPS displacement. The estimated parameters for this model are similar to those of "Model 0" and are consistent with the tectonic setting of the region.

### 5.3.4 Summary

As a result of the inversion, two new models were presented, one which best fitted the horizontal estimates of co-seismic displacement from this study and one which best fitted the measured uplift and subsidence observations reported by *Davies* (2002) and *Davies et al.* (2002). It was shown that a steep dipping thrust event along the NGT could explain the estimated GPS displacements. The evidence for this model being geophysically plausible, is somewhat inconclusive; mainly due to the limited interpretation of the region.

One thing that stands out between the two models estimated in this study is that the location of the fault tends to move west when the vertical constraints are applied, and east when the horizontal constraints are applied. This is clearly a result of the geometry of the observations. The observations of horizontal displacement are in the east and the

observations of uplift and subsidence were predominately made to the west. Due to insufficient data; the geometry of the GPS network could not be enhanced. However, if more observations of uplift, could be provided, in particular across the eastern end of the fault, a more representative model could be estimated.

To conclude that it was not possible to provide a single rupture that explained both the uplift and subsidence measurements and the horizontal GPS co-seismic displacements, a number of combined inversions were run. None of these models showed any significant improvement with estimates moving back and forth between either fitting the horizontal or the vertical observations. It is recommend that a further study be developed to look at the possibility of multiple ruptures across the boundary. A potential answer could be that the eastern part of the boundary ruptured in a steep dipping thrust event that displaced the GPS sites observed in this study, before triggering a second rupture to the west in a low angle thrust event (an hour latter to be consistent with local observations of uplift at Tarawai, Section 1.2.1).

# Conclusions and Recommendations

The intent of this thesis was to reconcile the previously published interpretation of PNG02 with estimates of surface displacement observed from the Global Positioning System. The study involved the analysis of GPS data to estimate earthquake deformation patterns, the interpretation and explanation of inter-seismic velocities and the inversion of co-seismic displacements to estimate fault geometry and slip parameters.

### Data Set Limitations

The data used in this study was obtained from a series of GPS campaigns between the years 2000 and 2005. All of the GPS sites observed in this network display some form of tectonic signal from PNG02. An aim of the study was to extract the co-seismic signal from the observed data. To do this, three levels of data reduction were required. Firstly, site positions relative to the ITRF2000 were estimated. The associated formal uncertainties are generally under-estimated (*Mao et al.*, 1999), hence they were multiplied by a factor of two (*Wallace et al.*, 2004). The interpretation of the uncertainties was an important step in the processing as error here had the potential to propagate throughout the reduction and subsequent inversion of displacements.

The second level of data reduction was to estimate inter-seismic velocities for each of the observed sites. This is where the first limitation of the data set was noticed. BAMI, MUTM, TARO, KOIL and XAVI only had multiple occupations after PNG02, hence estimated velocities had to be transferred from after the event to the single occupation before the event in order to compute the site location at the time of the earthquake. The reverse had to occur for the sites ANGR and TRNG. WEWK was the only site where observations were made both before and after the event. However, the calculated site velocities in the east component before and after PNG02 were significantly different. It was also noticed the observations made after PNG02 at XAVI displayed non-linear motion in the

east component and it was shown that this motion was the result of post-seismic relaxation. While XAVI and WEWK displayed a post-seismic signal, many of the other sites displayed inter-seismic signals from strain accumulation. All of these deformation signals had to be explained before the co-seismic displacements could be estimated.

Estimating co-seismic displacement was the final stage in the data reduction. The reliability of the co-seismic displacements was an important component of the analysis. The formal uncertainties provided for the co-seismic displacement did not provide the best indication of their reliability. These uncertainties were propagated through three levels of data reduction using, for the most part, simple linear propagation of errors. The resulting uncertainties were approximately four times larger than the estimated site position uncertainties. A much better way of interpreting the reliability of the co-seismic displacements was to look at the time between the last measurement before the event and the first measurement after the event. While it was not done in this study, future studies could develop a time based scale of reliability by which the co-seismic displacements could be weighted.

The co-seismic displacements were weighted in the non-linear inversion using a normalised uncertainty based on the magnitude of the displacement. This was done so that sites such as XAVI, which had displacement estimates an order of magnitude larger than the "far field" sites such as BAMI, did not dominate the inversion.

**A Reconciled Event?**

The main focus of this thesis was to reconcile the conflicting interpretation of the Wewak earthquake. The GPS observations showed displacements that were significantly different from displacements that were computed using the interpretation of *Borrero et al.* (2003). The model developed by *Borrero et al.* (2003) appears to only fit the observations of uplift and subsidence which were described by *Davies* (2002) and *Davies et al.* (2002). Co-seismic displacements estimated in this study were only calculated for the horizontal the components due to erratic observations in the vertical. Three sites which did provide reasonable observations of displacement in the vertical were XAVI which had a displacement of 33 cm that matches observed uplift on Kairiru of 35 cm, TRNG and WEWK. In an attempt to reconcile the observations I presented two "best" fitting models; a model based on only horizontal displacements and a model based on measurements of uplift

and subsidence.

The horizontal model was generated using just the estimated co-seismic displacements from the eight sites, ANGR, TRNG, WEWK, XAVI, BAMI, MUTM, KOIL and TARO. The result of this model was a rupture which provided a good fit to five sites, WEWK, TARO, KOIL, XAVI and TRNG. These are the sites that were observed immediately after the event; hence they have the most reliable estimates of co-seismic displacement. Comparisons were made using predicted vertical displacements. While the horizontal model provides a good fit to the observed horizontal displacements, it underestimates the uplift at the islands Tarawai and Walis and overestimates the subsidence along the northern coast of New Guinea. The model also shows a significant amount of subsidence in-between the islands Kairiru and Koil; there are no measurements in this region to confirm or refute the possibility of this subsidence.

The vertical model was constrained by using the observations of *Davies* (2002) and *Davies et al.* (2002) and also the observed GPS height changes at WEWK, XAVI and TRNG. This model accurately predicts uplift across the islands that is consistent with the measurements. Subsidence is also accurately predicted along the northern coast. However, the model does not accurately describe the horizontal GPS displacements.

In conclusion, neither of the presented models were successful in reconciling the conflicting data sets. If only GPS measurements were available the result would be a model which is described as a steep dipping thrust event with length 92 km, width 10 km, slip 3.3m and moment $2.32 \times 10^{27}$ dyne-cm which is equivalent to a moment magnitude of $M_w$ = 7.6. Is this model geophysically plausible? There are two elements of this solution that do raise some geophysical doubt. The first is that the location of the fault is shown to extend through the assumed location of the Bismarck Sea Seismic Lineation and that the dip angle is significantly larger, that assumed in the literature for the New Guinea Trench. As a result, both the horizontal and the vertical models fit different data sets. A recommendation for future studies would be to present a model describing a more complex rupture. A possible improvement on the rupture could be a 2-rupture model: the first a smaller rupture starting near the estimated location of "Model 2" and the second a larger rupture occurring in a location similar to that estimated for "Model 1".

**Tectonic Interpretation**

A significant component of this thesis was devoted to explaining the estimated GPS observations relative to the assumed a priori model for the area. The East Sepik region has been the subject of very few tectonic studies. This study therefore makes a significant contribution to the present tectonic description of the region. The geodetic network in this area strongly affected by a number of tectonic signals and there are only limited observations at the sites. While the observations are still inconclusive there is indication of the following:

- Velocity estimates at WEWK, TRNG, ANGR, ABTI, and MPRK appear to be consistently moving as a rigid block. In this study the rigid block has been referred to as Block "A". Between Block "A" and the rigid Australian Plate sit the New Guinea Highlands. A significant amount of uplift is occurring across this region which has been attributed to accommodation of the strain across the New Guinea Trench. Block A is observed to be moving slower than the Australian Plate, with the Australian Plate converging at a rate of $\sim$18 mm/yr. Such convergence could be causing uplift of the highlands.

- The site XAVI appears to be located on an isolated wedge between the NGT and BSSL. This has been assumed because the velocity estimate at XAVI does not fit any of the rigid plates, and the suggestion that BSSL runs east - west south of XAVI. This result is inconclusive and requires further investigation.

- Post-seismic relaxation appears to be occurring at WEWK and XAVI. This phase may also be causing non-linear motion at TARO and KOIL. It is not completely understood why KOIL and TARO are showing non-linear motion, but a number of suggestions have been made. From the exponential curves fitted to XAVI and WEWK, it appears that the post-seismic phase has a period of between 4 - 5 years.

**Suggestion of Future Developments and Studies**

Many of the interpretations made in this thesis has been inconclusive due to insufficient data. All the GPS sites used in this thesis are to be re-observed in November 2005. While these new observations will not significantly improve the estimated co-seismic displacements (this was observed by the inclusion of the 2005 data sets, where co-seismic es-

timated changed insignificantly), they will help to resolve some of the interpretations from this study that were left inconclusive due to insufficient data.

In terms of providing a better tectonic interpretation of the East Sepik region, I recommend that further observations be made in two areas (1) on the islands of Tarawai and Walis, and along the northern coast at But which does at present contain sufficient data to estimate a velocity. Such observations will help to validate the unusual velocity estimate at XAVI. (2) The network should also be extended further back into the New Guinea Highlands to either show support for the extension of the New Guinea Highlands Block in this area or delineate the motion of a separate block (Block "A"?).

This study concludes that it was possible to attribute the observed surface displacements to a single rupture, but it did not reconcile the GPS observations with the interpretation of *Borrero et al.* (2003). As such, this problem is still to be resolved. Further GPS measurements will not enhance the estimation of co-seismic displacements. Two suggestions which should be investigated are to re-process the GPS observations to extract more reliable height estimates which could be used to better constrain the eastern side of the rupture, and to attempt to combine the two models presented by this study using other sources of geodetic data, for example, Interferometric Synthetic Aperture Radar (InSAR).

# Bibliography

Beutler, G., E. Brockman, W. Gurtner, U. Hugentobler, L. Mervart, M. Rothacher, and A. Verdun (1994), Extended orbit modeling techniques at the code processing center of the internatioanl igs service for geodynamics (igs): Theory and initial results, *Manus. Geod.*, *19*(367-386).

Beutler, G., M. Rothacher, S. Schaer, T. A. Springer, J. Kouba, and R. E. Neilan (1999), The international gps service (igs): An interdisciplinary service in support of earth sciences, in *Satellite Dynamics, Orbit Analysis and Combination of Space Techniques*, *Advances in Space Research*, vol. 23, pp. 631–653, 4.

Bevis, M., and S. J. Martel (2001), Oblique plate convergence and interseismic strain accumulation, *Geochemistry Geophysics Geosystems*, *2*, art. no. 2000GC000,125.

Bock, Y., L. Prawirodirdjo, J. F. Genrich, C. W. Stevens, R. McCaffrey, C. Subarya, S. S. O. Puntodewo, and E. Calais (2003), Crustal motion in indonesia from global positioning system measurements, *Journal of Geophysical Research-Solid Earth*, *108*(B8).

Borrero, J. C., J. Bu, C. Saiang, B. Uslu, J. Freckman, B. Gomer, E. A. Okal, and C. E. Synolakis (2003), Field survey and preliminary modeling of the wewak, papua new guinea earthquake and tsunami of 9 september 2002, *Seismological Research Letters*, *74*(4), 393–403.

Chinnery, M. A. (1961), The deformation of ground around surface faults, *Bulletin of the Seismological Society of America*, *51*, 355–372.

Chlieh, M., J. B. de Chabalier, J. C. Ruegg, R. Armijo, R. Dmowska, J. Campos, and K. L. Feigl (2004), Crustal deformation and fault slip during the seismic cycle in the north chile subduction zone, from gps and insar observations, *Geophysical Journal International*, *158*(2), 695–711.

Cooper, P., and B. Taylor (1987), Seismotectonics of new-guinea - a model for arc reversal following arc-continent collision, *Tectonics*, *6*(1), 53–67.

Cox, A., and R. B. Hart (1986), *Plate Tectonics : how it works*, Palo Alto : Blackwell Scientific Publications.

Curtis, J. (1973), Plate tectonics of papua new guinea - solomon islands region, *Journal of the Geological Society of Australia*, *20*, 21–36.

Davies, H. (2002), Wewak earthquake and tsunami survey, *Tech. rep.*, International Tsunami Information Centre.

Davies, H., P. A. Symonds, and I. Ripper (1984), Strucutre and evolution of the solomon sea region, *Bureau of Mineral Resources Journal Australia*, *9*, 49–68.

Davies, H., C. Saiang, J. Bu, B. Uslu, C. Synolakis, J. Borrero, J. Freckman, and E. Okal (2002), The september 9, 2002 wewak, papua new guinea earthquake and tsunami, *Tech. rep.*, University of Southern California.

Davies, H. L., E. Honza, D. L. Tiffin, J. Lock, Y. Okuda, J. B. Keene, F. Murakami, and K. Kisimoto (1987), Regional setting and structure of the western solomon sea, *Geo-Marine Letters*, *7*(3), 153–160.

Davies, H. L., J. M. Davies, R. C. B. Perembo, and W. Y. Lus (2003), The aitape 1998 tsunami: Reconstructing the event from interviews and field mapping, *Pure and Applied Geophysics*, *160*(10-11), 1895–1922.

Delouis, B., et al. (2004), Slip distribution of the 2003 boumerdes-zemmouri earthquake, algeria, from teleseismic, gps, and coastal uplift data, *Geophysical Research Letters*, *31*(18), art. no. L18,607.

DeMets, C., R. G. Gordon, D. F. Argus, and S. Stein (1994), Effect of recent revisions to the geomagnetic reversal time-scale on estimates of current plate motions, *Geophysical Research Letters*, *21*(20), 2191–2194.

Denham, D. (1969), Distribution of earthquakes in new guinea-solomon islands region, *Journal of Geophysical Research*, *74*(17), 4290.

Dixon, T. H. (1991), An introduction to the global positioning system and some geological applications, *Reviews of Geophysics*, *29*(2), 249–276.

Dong, D., T. A. Herring, and R. W. King (1998), Estimating regional deformation from a combination of space and terrestrial geodetic data, *Journal of Geodesy*, *72*, 200–214.

Douglass, J., and B. Buffett (1995), The stress state implied by dislocation models of subduction deformation, *Geophysical Research Letters*, *22*(23), 3115–3118.

Everingham, I. (1974), Large earthquakes in new-guinea solomon-islands area, 1873-1972, *Tectonophysics*, *23*(4), 323–338.

Feigl, K. L., et al. (1993), Space geodetic measurement of crustal deformation in central and southern california, 1984-1992, *Journal of Geophysical Research-Solid Earth*, *98*(B12), 21,677–21,712.

Geller, R. C. (1975), Scaling relations for earthquake source parameters and magnitudes, *Bulletin of the Seismological Society of america*, *66*(5), 1501–1523.

Gutscher, M. A., W. Spakman, H. Bijwaard, and E. R. Engdahl (2000), Geodynamics of flat subduction: Seismicity and tomographic constraints from the andean margin, *Tectonics*, *19*(5), 814–833.

Hamilton, W. (1979), Tectonics of the indonesian region, *U.S. Geol. Surv. Prof.*, *Paper 1078*, 349.

Healy, D., N. Kusznir, and G. Yielding (2004), An inverse method to derive fault slip and geometry from seismically observed vertical stratigraphic displacements using elastic dislocation theory, *Marine and Petroleum Geology*, *21*(7), 923–932.

Hearn, E. (2003), What can gps data tell us about the dynamic of post-seismic deformation, *Geophysical Journal International*, *155*, 753–777.

Herring, T. A. (1999), Globk global kalman filter vlbi and gps analysis program, version 5.0, *Tech. rep.*, Mass. Inst. of Technol., Cambridge.

Hurukawa, N., Y. Tsuji, and B. Waluyo (2003), The 1998 papua new guinea earthquake and its fault plane estimated from relocated aftershocks, *Pure and Applied Geophysics*, *160*(10-11), 1829–1841.

Hyndman, R. D., and K. Wang (1995), The rupture zone of cascadia great earthquakes from current deformation and the thermal regime, *Journal of Geophysical Research-Solid Earth*, *100*(B11), 22,133–22,154.

Johnson, R. (1987), Delayed partial melting of subduction-modified magma sources in western melanesia: new results from the late cainozoic, in *Proceedings Pacific Rim Congress*, pp. 211–214, AusIMM, Melbourne.

Johnson, T., and P. Molnar (1972), Focal mechanisms and plate tectonics of southwest pacific, *Journal of Geophysical Research*, *77*(26), 5000–5032.

Kato, T., et al. (1998), Initial results from wing, the continuous gps network in the western pacific area, *Geophysical Research Letters*, *25*(3), 369–372.

Kim, Y. S., and D. J. Sanderson (2005), The relationship between displacement and length of faults: a review, *Earth-Science Reviews*, *68*(3-4), 317–334.

King, R., and Y. Bock (2000), Documentation for the gamit gps analysis software, release 10.0, *Tech. rep.*, Mass. Inst. of Technol., Cambridge.

Klootwijk, C., J. Giddings, C. Pigram, C. Loxton, H. Davies, R. Rogerson, and D. Falvey (2003), North sepik region of papua new guinea: palaeomagnetic constraints on arc accretion and deformation, *Tectonophysics*, *362*(1-4), 273–301.

Liu, P. (2005), Tsunami simulations and numerical models, *The Bridge*, *35*(2).

Mao, A. L., C. G. A. Harrison, and T. H. Dixon (1999), Noise in gps coordinate time series, *Journal of Geophysical Research-Solid Earth*, *104*(B2), 2797–2816.

McCaffrey, R. (2002), Crustal block rotations and coupling, in *Plate Boundary Zones*, edited by S. Stein and J. T. Freymueller, Geodynamic Series 30, pp. 101–122, American Geophysical Union.

McClusky, S., K. Mobbs, A. Stolz, D. Barsby, W. Loratung, K. Lambeck, and P. Morgan (1994), The papua new guinea satellite crustal motion surveys, *The Australian Surveyor*, *39*, 194–214.

McSaveney, M. J., J. R. Goff, D. J. Darby, P. Goldsmith, A. Barnett, S. Elliott, and M. Nongkas (2000), The 17 july 1998 tsunami, papua new guinea: evidence and initial interpretation, *Marine Geology*, *170*(1-2), 81–92.

Okada, Y. (1985), Surface deformation due to shear and tensile faults in a half-space, *Bulletin of the Seismological Society of America*, *75*(4), 1135–1154.

Okal, E. A. (1999), Historical seismicity and seismotectonic context of the great 1979 yapen and 1996 biak, irian jaya earthquakes, *Pure and Applied Geophysics*, *154*(3-4), 633–675.

Okal, E. A., and A. Cazenave (1985), A model for the plate tectonic evolution of the east-central pacific based on seasat investigations, *Earth and Planetary Science Letters*, *72*(1), 99–116.

Pegler, G., S. Das, and J. H. Woodhouse (1995), A seismological study of the eastern new-guinea and the western solomon sea regions and its tectonic implications, *Geophysical Journal International*, *122*(3), 961–981.

Puntodewo, S. S. O., et al. (1994), Gps measurements of crustal deformation within the pacific-australia plate boundary zone in irian-jaya, indonesia, *Tectonophysics*, *237*(3-4), 141–153.

Reilinger, R. E., et al. (2000), Coseismic and postseismic fault slip for the 17 august 1999, m=7.5, izmit, turkey earthquake, *Science*, *289*(5484), 1519.

Rizos, C. (1996), *Principles and Practice of GPS Surveying*, School of Geomatic Engineering, The University of New South Wales, Sydney Australia.

Ruegg, J. C., J. Campos, R. Madariaga, E. Kausel, J. B. de Chabalier, R. Armijo, D. Dimitrov, I. Georgiev, and S. Barrientos (2002), Interseismic strain accumulation in south central chile from gps measurements, 1996-1999, *Geophysical Research Letters*, *29*(11), art. no. 1517.

Sambridge, M. (1999a), Geophysical inversion with a neighbourhood algorithm - i. searching a parameter space, *Geophysical Journal International*, *138*(2), 479–494.

Sambridge, M. (1999b), Geophysical inversion with a neighbourhood algorithm - ii. appraising the ensemble, *Geophysical Journal International*, *138*(3), 727–746.

Sambridge, M. (2002), *Nonlinear inversion by direct search using the Neighbourhood Algorithm*, chap. IASPEI Handbook: Chapter 85.15, IASPEI.

Satake, K., and Y. Tanioka (2003), The july 1998 papua new guinea earthquake: Mechanism and quantification of unusual tsunami generation, *Pure and Applied Geophysics*, *160*(10-11), 2087–2118.

Savage, J. C. (1983), A dislocation model of strain accumulation and release at a subduction zone, *Journal of Geophysical Research*, *88*(NB6), 4984–4996.

Savage, J. C. (1996), Comment on, *Geophysical Research Letters*, *23*(19), 2709–2710.

Savage, J. C., and L. M. Hastie (1966), Surface deformation associated with dip-slip faulting, *Journal of Geophysical Research*, *71*, 4897–4904.

Savage, J. C., and J. L. Svarc (1997), Postseismic deformation associated with the 1992 m-w=7.3 landers earthquake, southern california, *Journal of Geophysical Research-Solid Earth*, *102*(B4), 7565–7577.

Savage, J. C., M. Lisowski, and W. H. Prescott (1991), Strain accumulation in western washington, *Journal of Geophysical Research-Solid Earth and Planets*, *96*(B9), 14,493–14,507.

Scholz, C. (2002), *The Mechanics of Earthquakes and Faulting, Second Ed.*, Cambrdige University Press.

Steketee, J. A. (1958), Some geophysical applications of the elasticity theory of dislocations, *Canadian Journal of Physics*, *36*(9), 1168–1198.

Stevens, C., R. McCaffrey, E. A. Silver, Z. Sombo, P. English, and J. van der Kevie (1998), Mid-crustal detachment and ramp faulting in the markham valley, papua new guinea, *Geology*, *26*(9), 847–850.

Tappin, D. R., P. Watts, G. M. McMurtry, Y. Lafoy, and T. Matsumoto (2001), The sissano, papua new guinea tsunami of july 1998 - offshore evidence on the source mechanism, *Marine Geology*, *175*(1-4), 1–23.

Tarantola, A. (2005), *Inverse Problem Theory and Methods for Model Parameter Estimation*, Society for Industrial and Applied Mathematics, Philapelphia.

Taylor, B. (1979), Bismarck sea: evolution of a back-arc basin, *Geology*, *7*(171-174).

Tregoning, P. (2002), Plate kinematics in the western pacific derived from geodetic observations, *Journal of Geophysical Research-Solid Earth*, *107*(B1), art. no. 2020.

Tregoning, P., and A. Gorbatov (2004), Evidence for active subduction at the new guinea trench, *Geophysical Research Letters*, *31*(13), art. no. L13,608.

Tregoning, P., R. J. Jackson, H. McQueen, K. Lambeck, C. Stevens, R. P. Little, R. Curley, and R. Rosa (1999), Motion of the south bismarck plate, papua new guinea, *Geophysical Research Letters*, *26*(23), 3517–3520.

Tregoning, P., H. McQueen, K. Lambeck, R. Jackson, R. Little, S. Saunders, and R. Rosa (2000), Present-day crustal motion in papua new guinea, *Earth Planets and Space*, *52*(10), 727–730.

Tregoning, P., et al. (1998), Estimation of current plate motions in papua new guinea from global positioning system observations, *Journal of Geophysical Research-Solid Earth*, *103*(B6), 12,181–12,203.

Wallace, L. M., et al. (2004), Gps and seismological constraints on active tectonics and arc-continent collision in papua new guinea: Implications for mechanics of microplate rotations, *Journal of Geophysical Research-Solid Earth*, *109*(B5), art. no. B05,404.

Weissel, J. K., and R. N. Anderson (1978), Is there a caroline plate, *Earth and Planetary Science Letters*, *41*(2), 143–158.

Williams, C. A., and R. McCaffrey (2001), Stress rates in the central cascadia subduction zone inferred from an elastic plate model, *Geophysical Research Letters*, *28*(10), 2125–2128.

Zhao, S. R., and S. Takemoto (2000), Deformation and stress change associated with plate interaction at subduction zones: a kinematic modelling, *Geophysical Journal International*, *142*(2), 300–318.

# Vertical Displacements

Some of the GPS time series show erratic variations in the heights, most likely caused by errors in antenna height measurements used in the reduction of the GPS observations (not all field notes were available to verify these values). The time series at WEWK, XAVI and TRNG are reasonably consistent and clear co-seismic displacements can be identified.

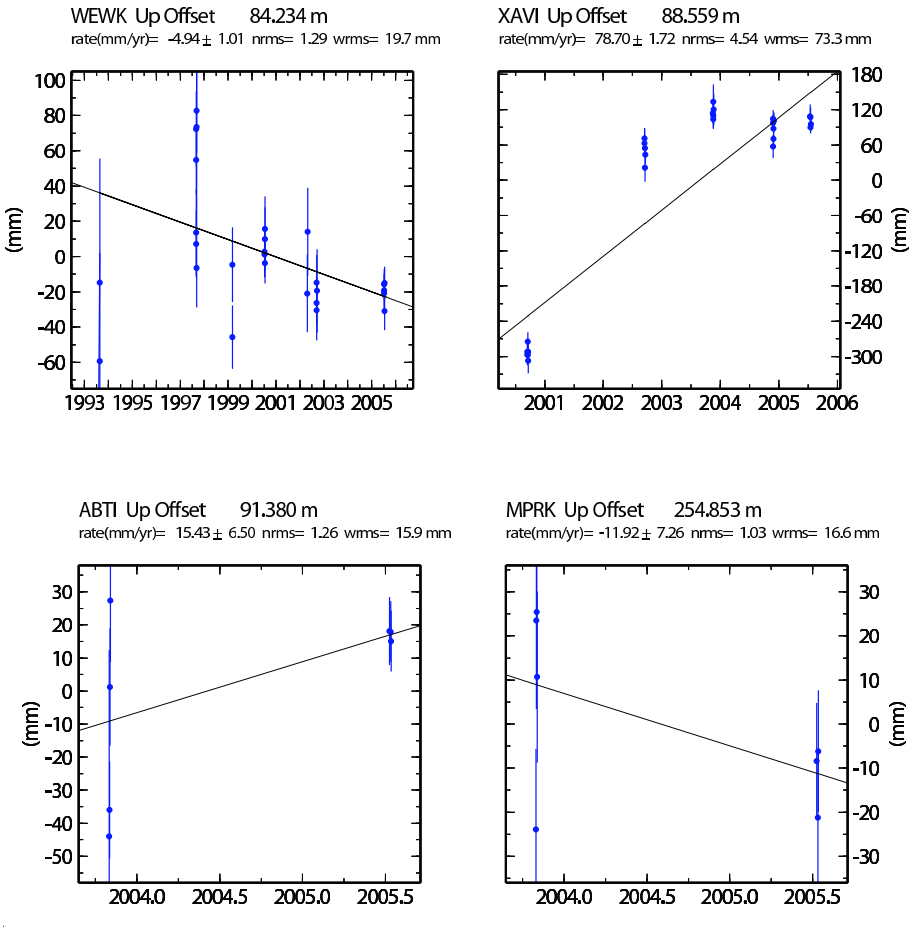


**Figure A.1**: Vertical time series produced in the GLOBK analysis (continued).

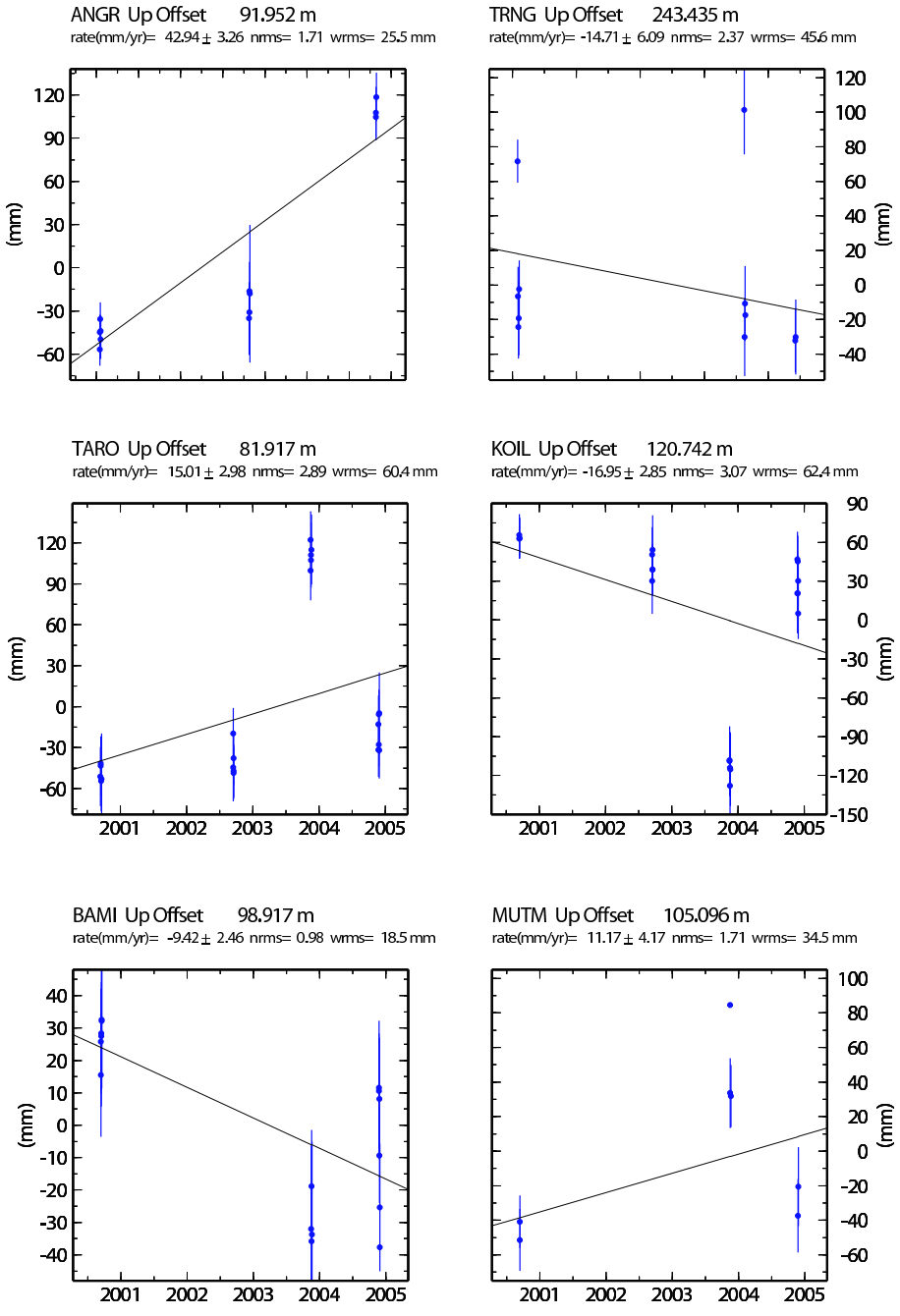
ANGR Up Offset 91.952 m
rate(mm/yr)= 42.94 ± 3.26 nrms= 1.71 wrms= 25.5 mm
TRNG Up Offset 243.435 m
rate(mm/yr)= -14.71 ± 6.09 nrms= 2.37 wrms= 45.6 mm
TARO Up Offset 81.917 m
rate(mm/yr)= 15.01 ± 2.98 nrms= 2.89 wrms= 60.4 mm
KOIL Up Offset 120.742 m
rate(mm/yr)= -16.95 ± 2.85 nrms= 3.07 wrms= 62.4 mm
BAMI Up Offset 98.917 m
rate(mm/yr)= -9.42 ± 2.46 nrms= 0.98 wrms= 18.5 mm
MUTM Up Offset 105.096 m
rate(mm/yr)= 11.17 ± 4.17 nrms= 1.71 wrms= 34.5 mm
(mm)
2001
2002
2003
2004
2005

# Elastic Dislocation in a Finite Rectangular Half Space

The *Okada* (1985) model for estimation of elastic dislocation in a finite rectangular half-space was provided in the form of a fortran subroutine (SRECTF.f), this code uses the following equations to calculate elastic displacements.

For Strike Slip:

$$U_x = -\frac{U_1}{2\pi}\left[\frac{\xi q}{R(R+\eta)} + atan\frac{\xi\eta}{qR} + I_1 sin\delta\right] \|$$

$$U_y = -\frac{U_1}{2\pi}\left[\frac{yq}{R(R+\eta} + \frac{qcos\delta}{R+\eta} + I_2 sin\delta\right] \|$$

$$U_z = -\frac{U_1}{2\pi}\left[\frac{dq}{R(R+\xi} + sin\delta atan\frac{\xi\eta}{qR} - I_5 sin\delta cos\delta\right] \|$$

For Dip-Slip:

$$U_x = -\frac{U_2}{2\pi}\left[\frac{q}{R} - I_3 sin\delta cos\delta\right] \|$$

$$U_y = -\frac{U_2}{2\pi}\left[\frac{yq}{R(R+\xi)} + cos\delta atan\frac{\xi\eta}{qR} - I_1 sin\delta cos\delta\right] \|$$

$$U_z = -\frac{U_2}{2\pi}\left[\frac{dq}{R(R+\xi)} + sin\delta atan\frac{\xi\eta}{qR} - I_5 sin\delta cos\delta\right] \|$$

For Tensile:

$$U_x = \frac{U_3}{2\pi}\left[\frac{q^2}{R(R+\eta)} - I_3 sin^2\delta\right] \|$$

$$U_y = \frac{U_3}{2\pi}\left[\frac{-dq}{R(R+\xi)} - sin\delta(\frac{\xi q}{R(R+\eta)} - atan\frac{\xi\eta}{qR}) - I_1 sin^2\delta\right] \|$$

$$U_z = \frac{U_3}{2\pi}\left[\frac{yq}{R(R+\xi)} + cos\delta(\frac{\xi q}{R(R+\eta)} - atan\frac{\xi\eta}{qR}) - I_5 sin^2\delta\right] \|$$

# Displacement at KOIL and TARO

In section 4.2.1 the possibility of a second co-seismic displacement at the sites KOIL and TARO was discussed to explain the observed non-linear motion. Figure C.1 shows the evidence the resulting time series if such a displacment was present. Figure C.2 shows the displacement field that would be required to fit the observed co-seismic displacements.

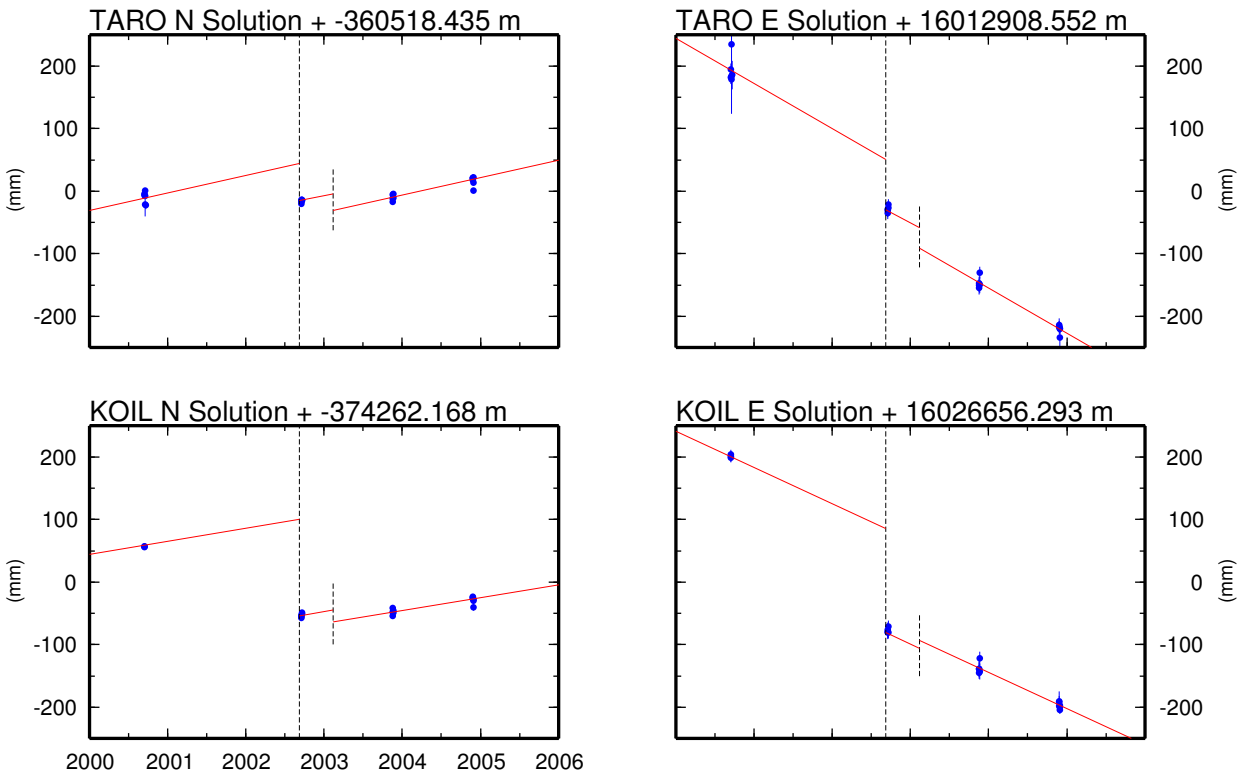


**Figure C.1**: Possible co-seismic displacements at KOIL and TARO after PNG02.

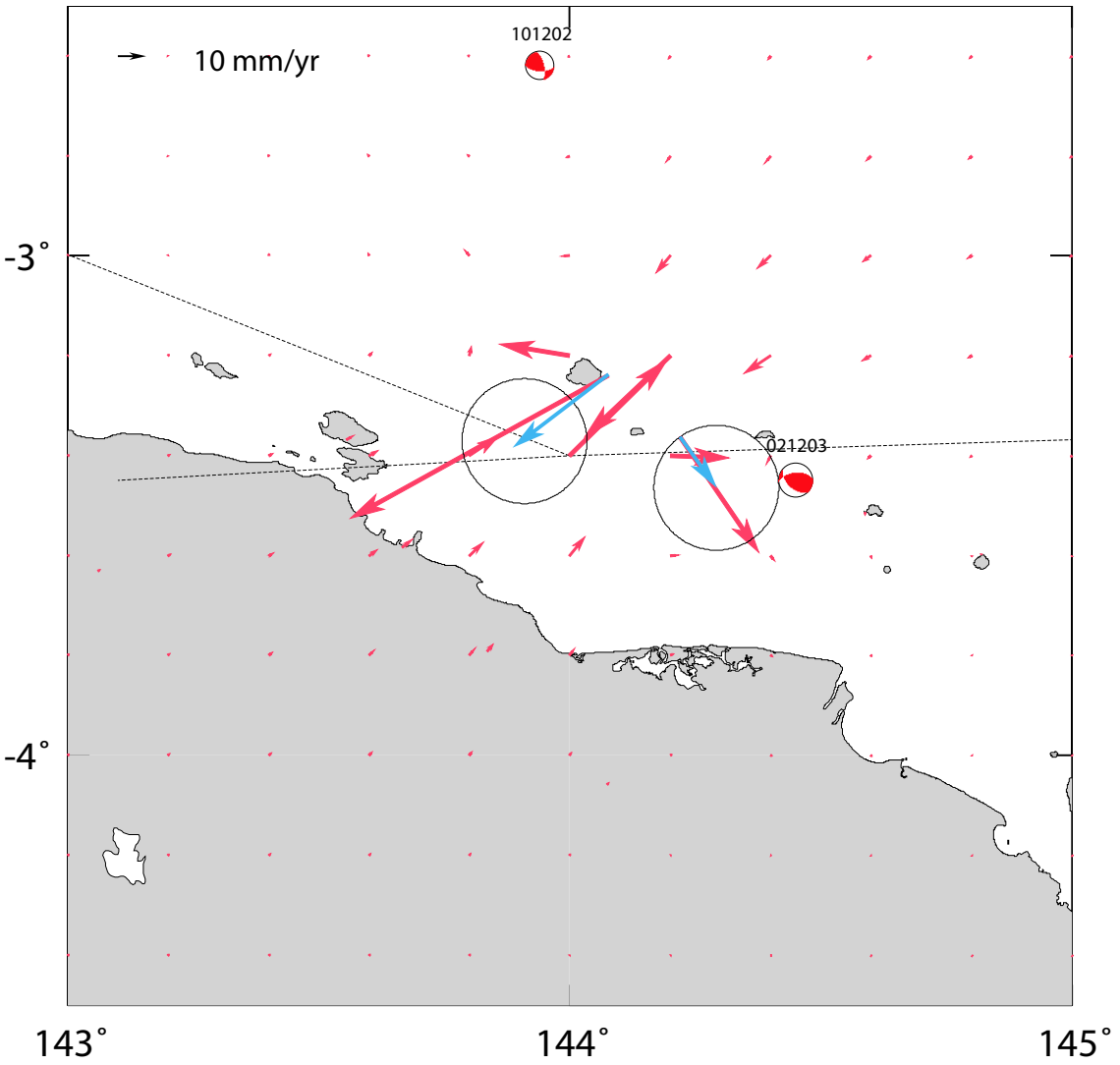


**Figure C.2:** Elastic dislocation pattern (red) that would be required to explain the possible second co-seismic displacements at TARO and KOIL (blue). Also shown are the Harvard CMT focal mechanisms for the three events that occured during this period.

# Elastic Dislocation Models

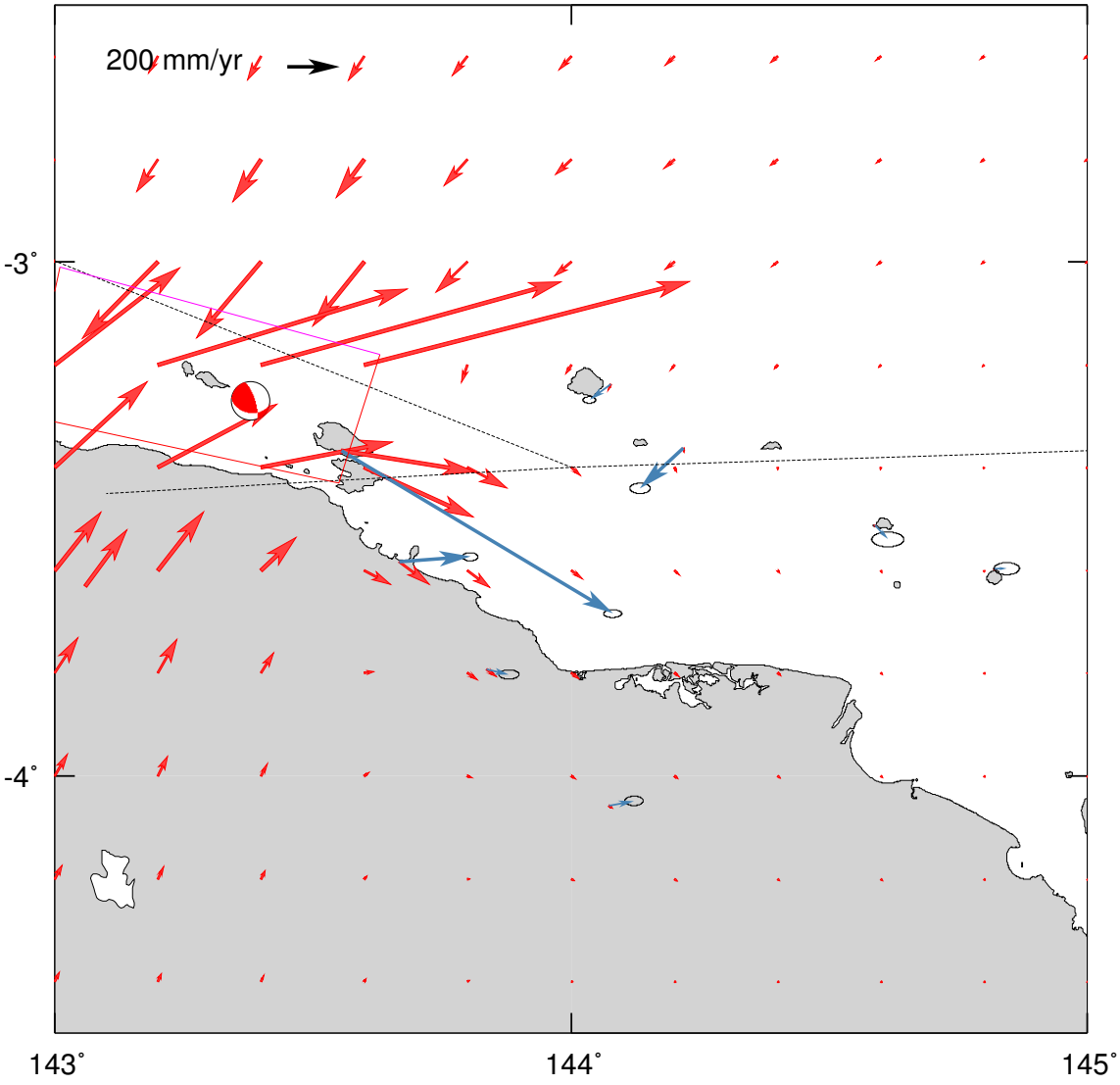


**Figure D.1:** Complete elastic dislocation model. (a) Replication of the model described by *Borrero et al.* (2003).

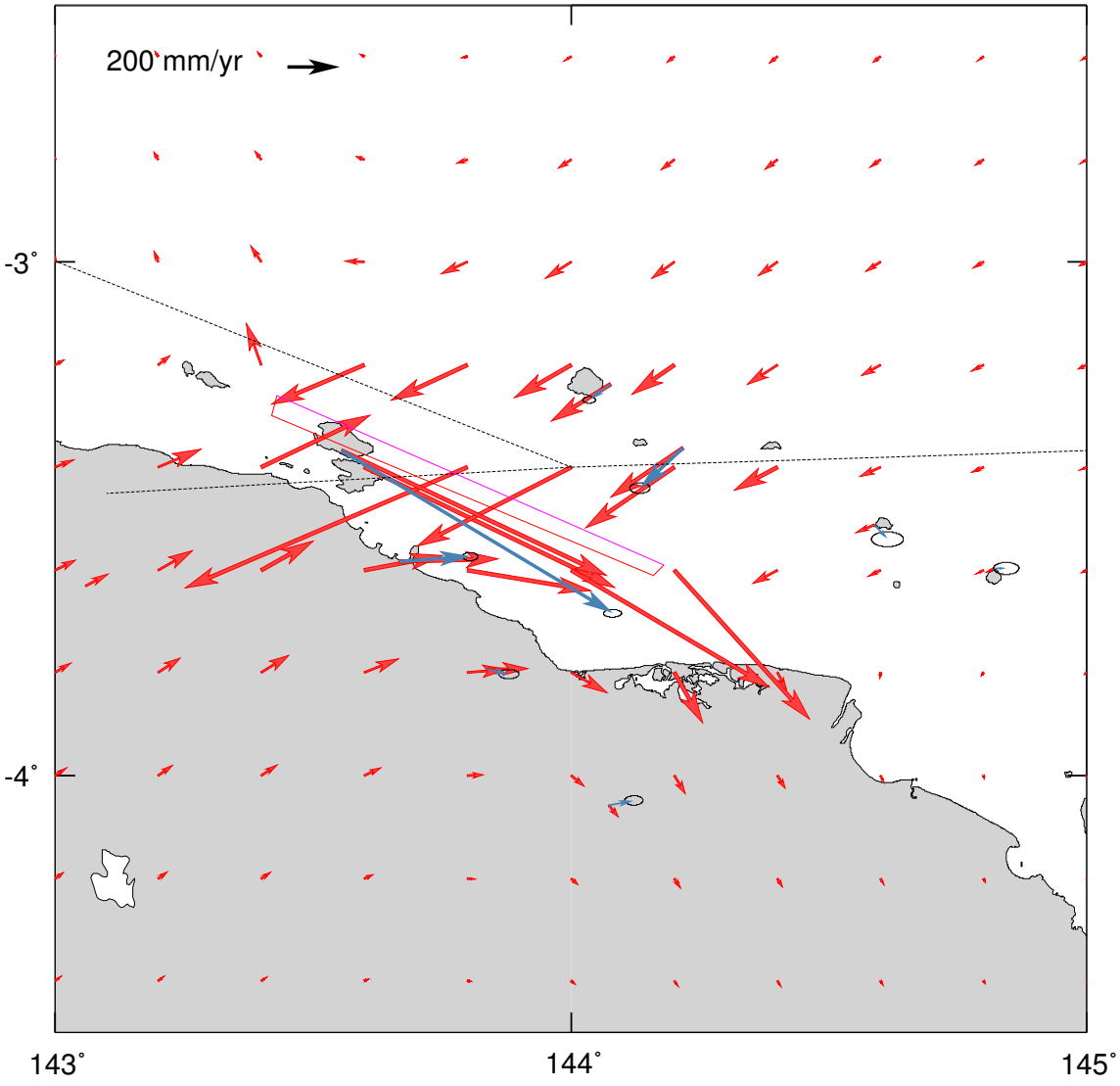


**Figure D.2:** Complete elastic dislocation model. (b) Inversion Model 1 - GPS Dispalcement Model.

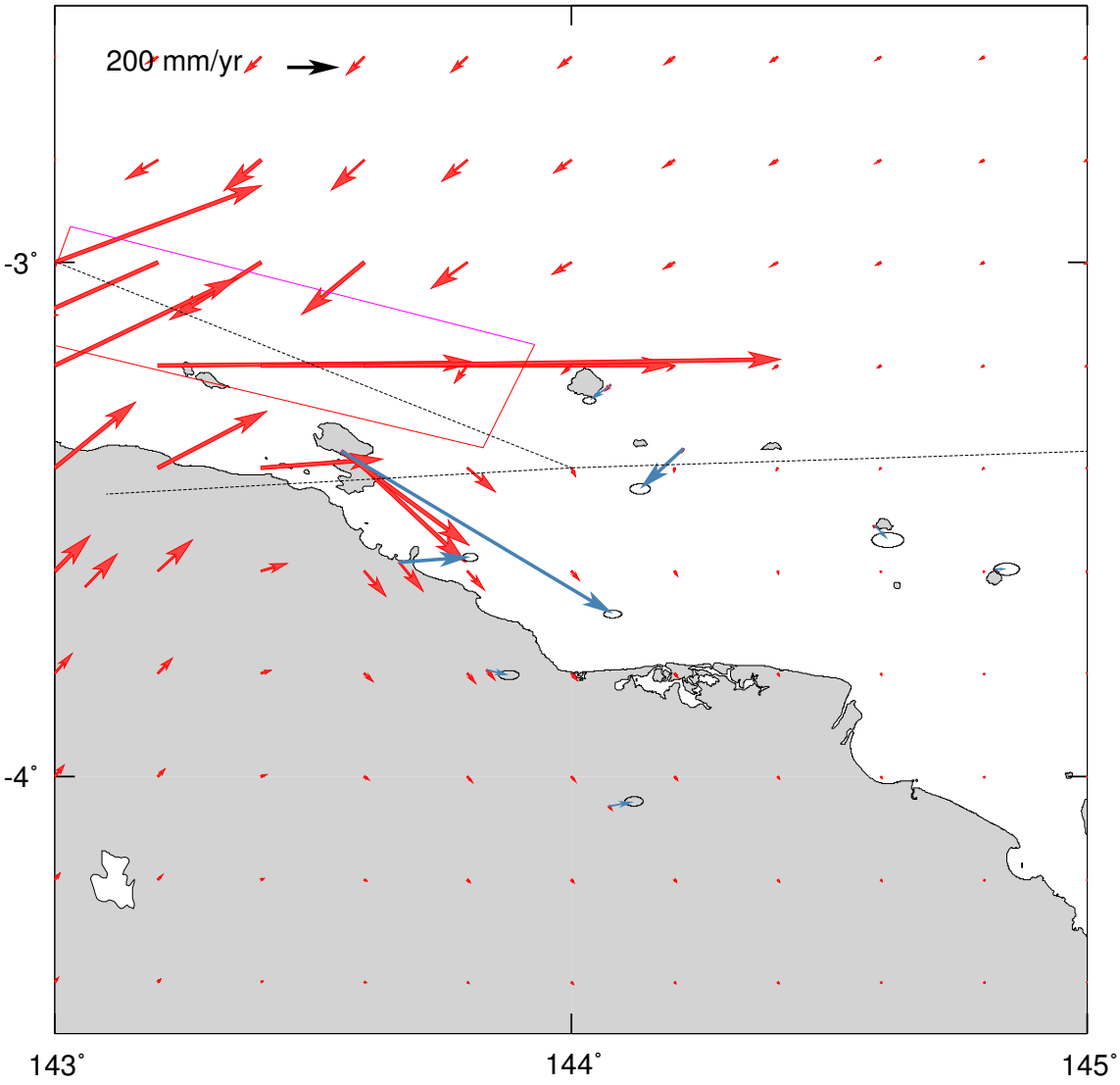


**Figure D.3:** Complete elastic dislocation model. (c) Inversion Model 2 - Vertical Displacement Model.